INTERACTION NOTES

NOTE 455

21 November 1985

A Calculational Model of Corona Effects on a Conducting Wire in a High Altitude Electromagnetic Pulse (HEMP) Environment*

J.P. Blanchard
LuTech, Inc.
3742 Mount Diablo Boulevard
Lafayette, CA 94549

Abstract

This note extends the work of Dr. Carl Baum, in Interaction Note #441, on corona formation around conducting lines in an HEMP environment to examine the impact of corona on line currents. Various parameters of the model are analyzed for their impact on corona formation in terms of an experiment proposed to verify the results of the model. Guidelines for the design of that experiment are proposed in terms of the parameters examined.

* Research sponsored by the office of Energy Storage and Distribution, US Department of Energy, and was performed under subcontract number 19X-027461C with Martin Marietta Energy Systems, Inc.

SEE LETTER IN BACK

INTERACTION NOTES

NOTE 455

21 November 1985

A Calculational Model of Corona Effects on a Conducting Wire in a High Altitude Electromagnetic Pulse (HEMP) Environment*

J.P. Blanchard
LuTech, Inc.
3742 Mount Diablo Boulevard
Lafayette, CA 94549

Abstract

This note extends the work of Dr. Carl Baum, in Interaction Note #443, on corona formation around conducting lines in an HEMP environment to examine the impact of corona on line currents. Various parameters of the model are analyzed for their impact on corona formation in terms of an experiment proposed to verify the results of the model. Guidelines for the design of that experiment are proposed in terms of the parameters examined.

* Research sponsored by the office of Energy Storage and Distribution, US Department of Energy, and was performed under subcontract number 19X-027461C with Martin Marietta Energy Systems, Inc.

ACKNOWLEDGEMENTS

The work related to this project is being done under subcontract number 19X-027461C from Oak Ridge National Laboratory. I would like to thank Dr. Carl Baum and Dr. F.M. Tesche for helpful discussions pertaining to this task.

I. INTRODUCTION

Corona is induced when the electric field normal to a conducting line exceeds the dielectric strength of the surrounding material. Massive ionization begins to occur in the surrounding material and a coaxial sheath of free charges appears around the line. The radius of this sheath is determined by the point at which the local electric field can no longer support ionization of the medium.

Corona effects on a conducting wire have been studied for many years [1,2,3,4,5] when the line was excited either by injecting a current pulse on the wire [6,7] or by illumination with an appropriate electromagnetic field with a fairly slow rise time [8,9]. A typical HEMP (High altitude ElectroMagnetic Pulse) field has a faster rise time than waves considered in previous corona studies. In addition, the response of a conducting line subject to an incident EMP field is more appropriately modelled by a series of distributed sources on a transmission line [10] than by the injected pulse model used previously [5].

Several corona models have been proposed for lines subject to EMP fields [11]. This memo presents the results of a calculation model of corona effects on a line with an incident EMP plane wave based upon a transmission line model described by Dr. Carl Baum [12]. In this model, the per-unit-length capacitance between the conducting line and an effective reference conductor (whose definition is based upon experiment geometry) is altered by the presence of corona, reducing the current seen on the line from the value expected without corona.

Baum's model considers corona effects on an infinite line in terms of a normalized charge-per-unit-length. In the present paper, the normalized results of his model are extended to obtain expected line current as a function of time. Based upon this, an experiment is being considered to test the effects of corona (in terms of current responses) on a line excited by an HEMP field. This report serves to define the geometry and expected current responses for the experiment.

After postulating an experiment geometry, the effects of varying some of the parameters of the model are discussed. Consideration is then given to experimental limitations. The infinite line assumption in Baum's model is appropriate only for a limited time (i.e. the clear time) before reflections from the line ends interfere with local corona observations. Studies of variation of current with test wire length are presented in connection with clear time calculations.

Because of the large number of electrical and physical parameters involved in the generation of corona, several assumptions and simplifications have been made in this study. Some of these are discussed in the summary of this report. The final test of the validity of these assumptions will be the experiment measuring corona effects discussed here.

II. CORONA MODEL

Figure 1 shows an E-field incident at an angle a upon a conducting wire of radius r_o. If the normal component of the incident E-field is sufficiently large, a corona of radius r_c forms. An effective reference conductor of radius r_∞ surrounds the conducting wire as shown.

Equivalent transmission line models of a conducting line with induced corona are shown in Figures 2 and 3. (As discussed in [12], the case of a wire in free space and the case of a wire above an infinitely conducting ground plane may be treated in the same manner provided the geometry is appropriately defined.) When the corona conductivity is sufficiently high (a reasonable assumption since corona is comprised of highly ionized gas), the circuit model of Figure 3.a. reduces to that of Figure 3.b.

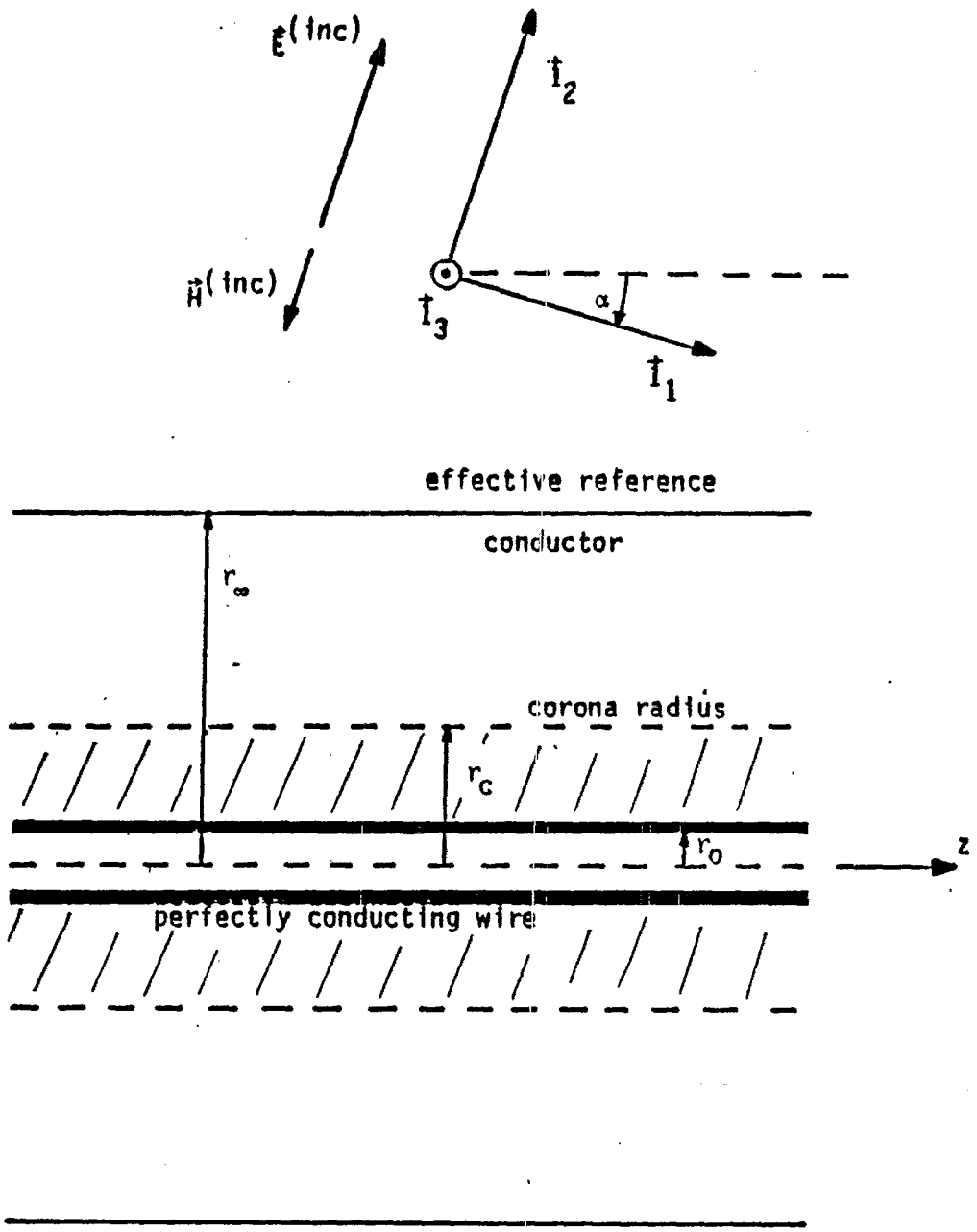

Figure 1. Corona Model of Infinite Wire in Free Space [12]

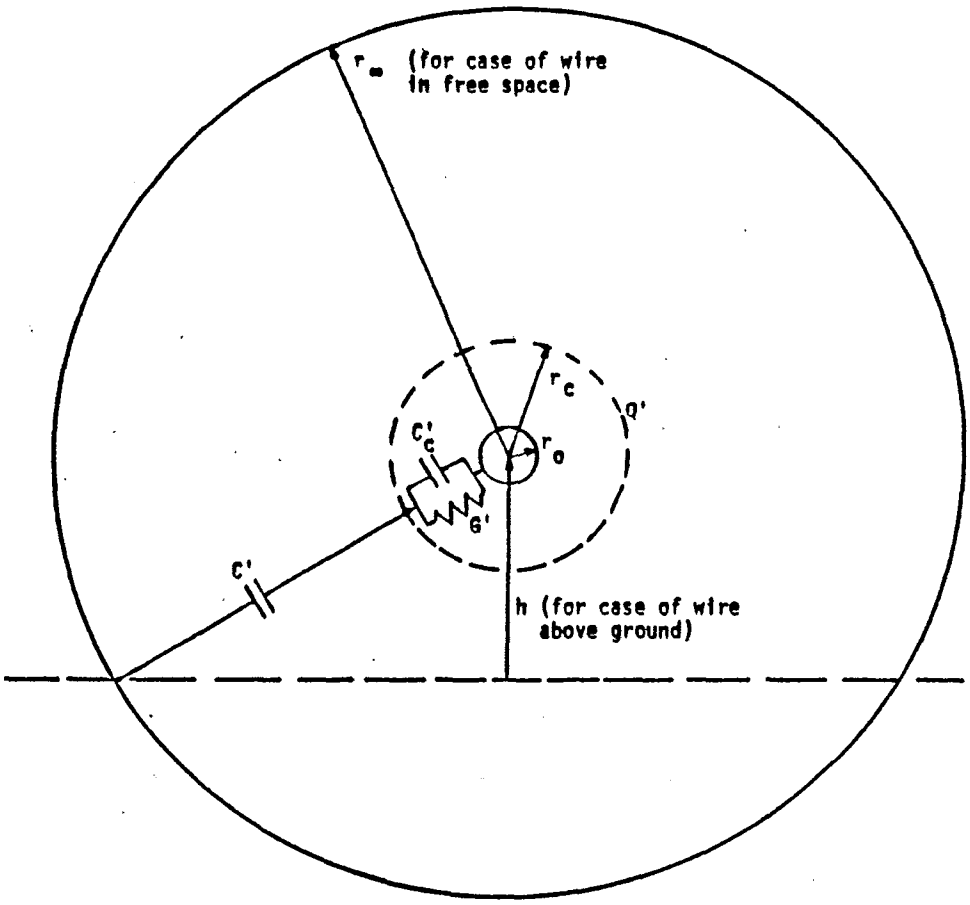

Figure 2. Equivalent Corona Radius Model [12]

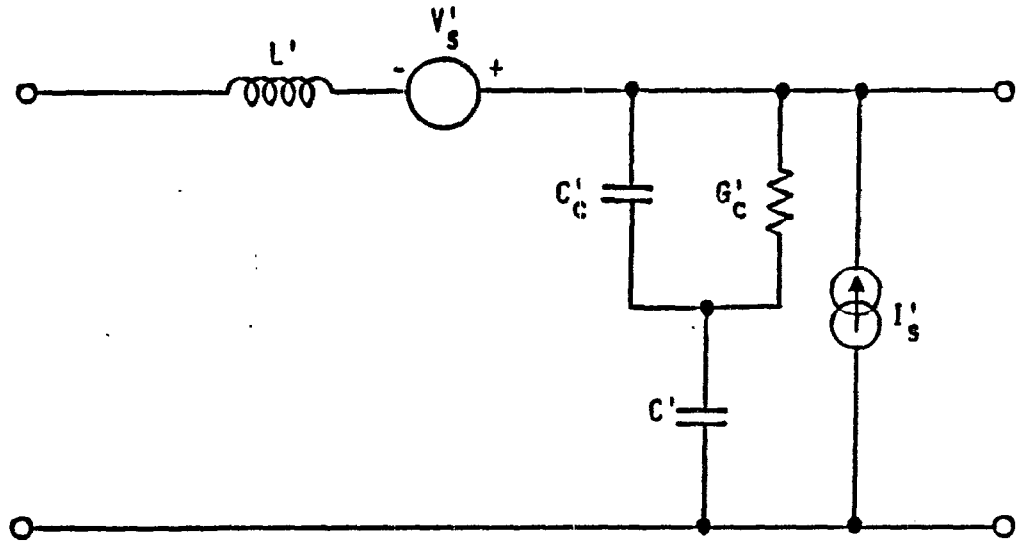

A. General case with uniform corona

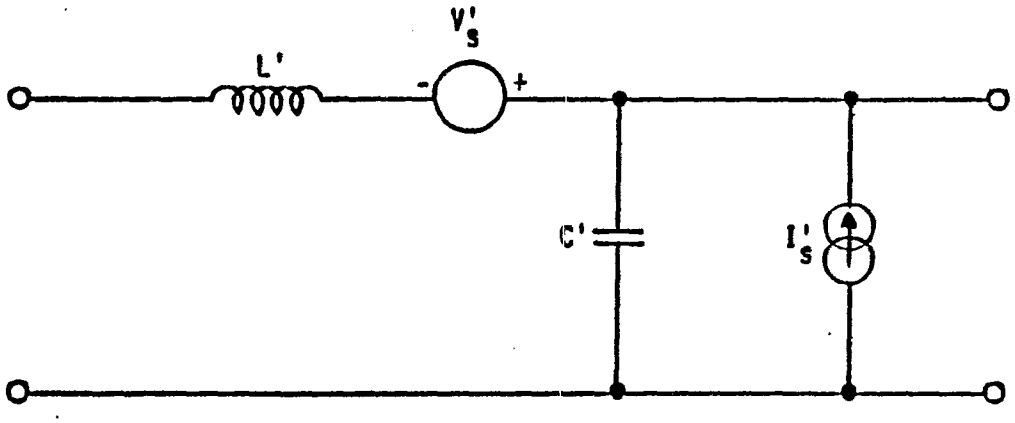

B. Case with sufficiently large corona conductivity

Figure 3. Per-Unit-Length Transmission-Line Equivalent Circuit Representation [12]

The circuit in Figure 3.b is described by the following telegrapher's equations:

$$\frac{\partial V}{\partial z} = - L' \frac{\partial I}{\partial t} + V_s' \qquad (1)$$

$$\frac{\partial I}{\partial z} = - \frac{\partial}{\partial t} (C'V) + I_s' \qquad (2)$$

$C' = C'(Q') = \frac{Q'}{V}$ = capacitance per unit length

Q' = charge per unit length

L' = inductance per unit length

V_s' = longitudinal voltage source per unit length

I_s' = transverse current source per unit length

Choosing an appropriate path of integration, these equations can be simplified to

$$\frac{\partial}{\partial z} \left[\frac{Q'}{C'}\right] = -L' \frac{\partial I}{\partial t} + E_t \qquad (3)$$

$$\frac{\partial I}{\partial z} = - \frac{\partial Q'}{\partial t} \qquad (4)$$

where E_t is the tangential component of the local electric field.

Choosing a plane wave excitation of the line, equations (3) and (4) assume the form

$$-\frac{1}{v_p}\frac{Q'}{C\tau} + v_p L'Q' = \int_{-\infty}^{\tau} E_t(\tau')\, d\tau'$$

$$\equiv E_1\, g(\tau) \qquad (5)$$

with

$$v_p = \frac{c}{\cos(\alpha)} \qquad (6a)$$

$$E_t = E_0 f(t - \frac{z}{v_p}) \sin(\alpha) \qquad (6b)$$

$$\tau \equiv t - \frac{z}{v_p} \qquad (6c)$$

$$g(\tau) \equiv \int_{-\infty}^{\tau} f(\tau')\, d\tau' \qquad (6d)$$

$$\int_{-\infty}^{\tau} E_t(\tau')\, d\tau' = E_1 g(\tau) \qquad (6e)$$

$$E_1 = E_0 \sin(\alpha). \qquad (6f)$$

Neglecting the effects of corona, the line capacitance remains constant, and equation 5 simplifies to

$$Q'(\tau) = \left\{-\cos(\alpha) + \frac{1}{\cos(\alpha)}\right\}^{-1} \frac{1}{Z_{c_o}} E_1 g(\tau) \tag{7}$$

with

$$Z_{c_o} = f_{g_o} Z_o \qquad \text{(characteristic impedance)} \tag{8}$$

$$f_{g_o} = \frac{1}{2\pi} \ln\left(\frac{r_\infty}{r_o}\right) \qquad \text{(for infinite line in free space)} \tag{8a}$$

$$f_{g_o} = \frac{1}{2\pi} \operatorname{arccosh}\left(\frac{h}{r_o}\right) \qquad \text{(for infinite line at a height, h, above a ground plane)} \tag{8b}$$

When corona occurs, the capacitance of the line is altered and direct solution of equation 5 becomes difficult. Solving for the local charge per unit length, Q'(t), one obtains the parametric equation

$$\left\{-\cos(\alpha) + \frac{1}{\cos(\alpha)} + \cos(\alpha) \frac{\ln \frac{|Q'(\tau)|}{Q'_o}}{\ln\left(\frac{Q'_\infty}{Q'_o}\right)}\right\} \frac{Q'(\tau)}{Q'_o} = \frac{E_1 g(\tau)}{Z_{c_o} Q'_o} \tag{9}$$

when $\dfrac{|Q'(\tau)|}{Q'_o} \geq 1$

with $Q'_o = 2\pi\varepsilon_o r_o E_b$ (10)

(For $|Q'(t)| < Q'_o$, the capacitance is assumed unaltered, and equation 7 applies.).

As discussed by Baum [12], $I(t) = Q_o'(t) * v_p$ (where v_p is the wave phase velocity defined in equation (6a)). Equations (7) and (9) transform to

$$I(\tau) = \left\{-\cos(\alpha) + \frac{1}{\cos(\alpha)}\right\}^{-1} \frac{cE_1 g(\tau)}{Z_{c_o} \cos(\alpha)} \tag{11}$$

$$\left[-\cos(\alpha) + \frac{1}{\cos(\alpha)} - \frac{\cos(\alpha)}{2\pi f_{g_o}} \ln\left(\frac{Q_o' c}{\cos(\alpha)}\right) + \frac{\cos(\alpha)}{2\pi f_{g_o}} \ln\left(|I(\tau)|\right)\right] I(\tau) = \frac{cE_1 g(\tau)}{Z_{c_o} \cos(\alpha)} \tag{12}$$

respectively.

III. EXPERIMENT GEOMETRY

An experiment to test this model is diagrammed in Figure 4. A test conductor wire is strung from the top of an EMP simulator called VPD (Vertically Polarized Dipole; also known as ATHAMAS II (AFWL Terrestrial HEMP Alert Mode Aircraft Simulator)) diagonally down to the ground plane. An observation point is chosen somewhere along this wire. The optimum location of this observation point will be discussed in section V. Although the wave fronts emanating from the VPD are essentially spherical, at a sufficient distance from the source they may be considered locally planar. Note that the local angle of E-field incidence with the wire at an observation point, α, is typically different from the angle the wire makes with the ground plane, ϕ. The dashed lines below the ground plane indicate an image of the experiment setup that is the electrical equivalent of the ground plane shown.

For the purposes of the calculations in this memo, the VPD is assumed to have a slant height, L, of 53 meters and a cone half angle of 41^{o}. (These values are quite close to the actual mechanical and electrical specifications for VPD given in references [13,14].) These correspond to a vertical VPD height of 40 meters. Hence, a test conductor in this configuration could not be less than 40 meters.

The next section examines the impact of changes in some of the model parameters in light of this experiment design.

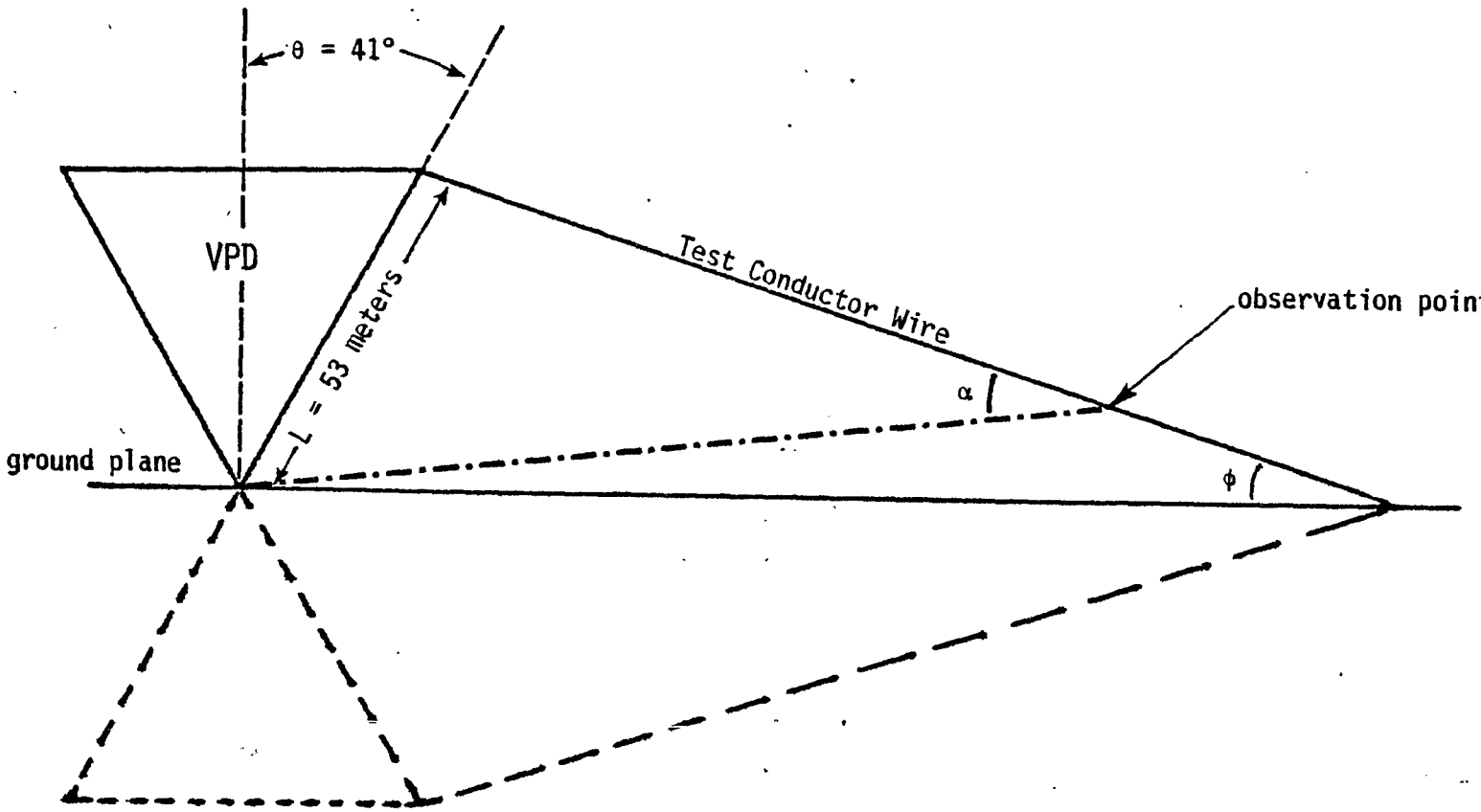

Figure 4. Experiment Setup

IV. DISCUSSION OF EQUATION PARAMETERS

Examining equations (11) and (12), model parameters which could vary are τ, α, $E_1 g(\tau)$, Z_{c_0}, f_{g_0}, and Q_0'. From equations (8,8a,8b), Z_{c_0} is directly proportional to f_{g_0} with proportionality constant Z_0, the impedance of free space. Hence, variations in Z_{c_0} are the same as variations in f_{g_0}. From equation (10), the corona charge-per-unit-length, Q_0', is directly proportional to the radius of the test conductor, r_0, which is a more directly measurable parameter.

This experiment will be concerned with the response of the test conductor to a time varying E-field as measured by the time varying current, $I(\tau)$, seen on the wire. From the discussion above, the unique parameters that may vary in this model are τ (retarded time), α (angle of E-field incidence with the test conductor wire), $E_1 g(\tau)$ (from equation (5), a measure of the time varying incident E-field), f_{g_0} (discussed in detail below), and r_0 (test conductor radius). In each subsection below, one of these parameters will be varied (beginning with the $E_1 g(\tau)$ and followed, respectively, by r_0, f_{g_0}, and α) to determine its impact on expected model results in the experiment configuration described earlier. Default values (i.e. values used implicitly) for parameters not being examined are summarized in Table 1.

Angle of incidence = 36 degrees

$E_1 g(\tau)$ as shown in Figure 5.

f_{g_0} = 1.0 (This corresponds to an observation point ~ 2.68 meters above the ground plane for a wire of radius 1.0 cm.)

Conductor wire radius, r_0 = 0.01 meters = 1.0 centimeters

TABLE 1 : DEFAULT PARAMETERS

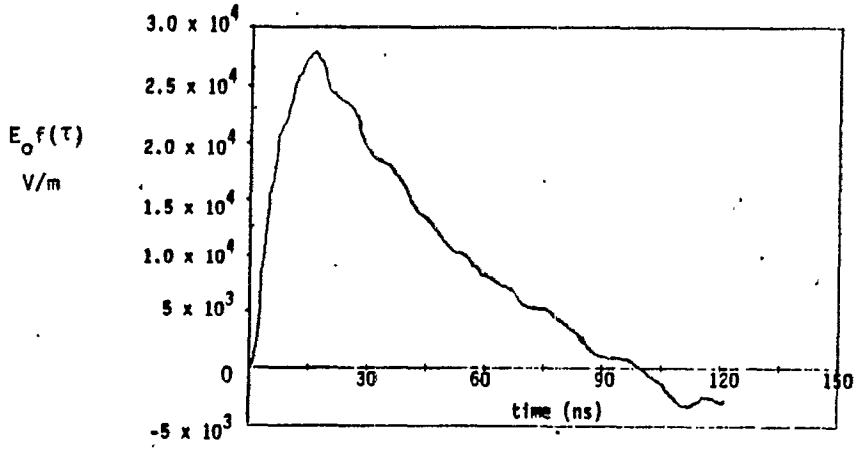

Figure 5a. VPD E-field as measured 100 meters laterally from base of VPD and 20 meters above ground plane.

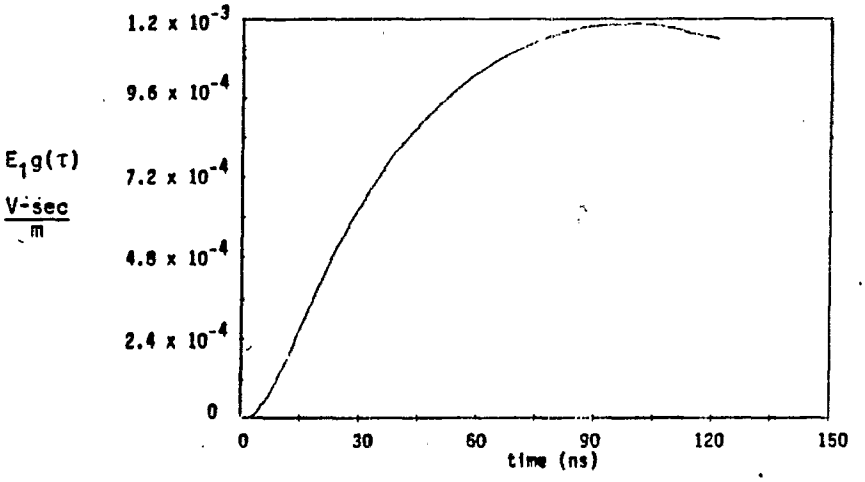

Figure 5b. Integrated VPD E-field from Figure 5a.

A. $E_{breakdown}$; $E_1 g(\tau)$

From equation (5), $E_1 g(\tau)$ is, in some sense, a measure of the local time-varying E-field incident upon the wire. This incident E-field generates a current on the test line and it is the local E-field due to the current on the test line that may generate corona. Without the current excited on the line, the E-field from the the pulser would be insufficient to cause corona. This is why corona is seen only in the vicinity of local conductors and not throughout the rest of the pulser work volume. If the local E-field due to the current on the line exceeds the maximum E-field value the air can support, $E_{breakdown}$, corona (consisting of a coaxial sheath of ionized air molecules) forms around the wire. $E_{breakdown}$, or E_b, is also called the dielectric strength of the medium; for air, $E_b \approx 3 \times 10^6$ [15]. Since the magnitude of the driving E-field varies as (1/R), corona is less likely to form for points farther away from the source.

B. Conductor Radius

Figures 6a and 6b demonstrate how changes in wire radius are reflected in both the magnitude of the line current and in the corona onset time. Figure 6a compares the late time responses of wires of different radii, while Figure 6b shows the early time responses, where differences in corona onset times are more apparent. Corona onset times for various wire radii are summarized in Table 2.

WIRE RADIUS	CORONA ONSET TIME (ns)
1/2 inch	27.7
1.0 cm	22.3
1/4 inch	15.9
1/8 inch	10.4
1/16 inch	7.11

TABLE 2 : CORONA ONSET TIMES WITH VARYING WIRE RADIUS

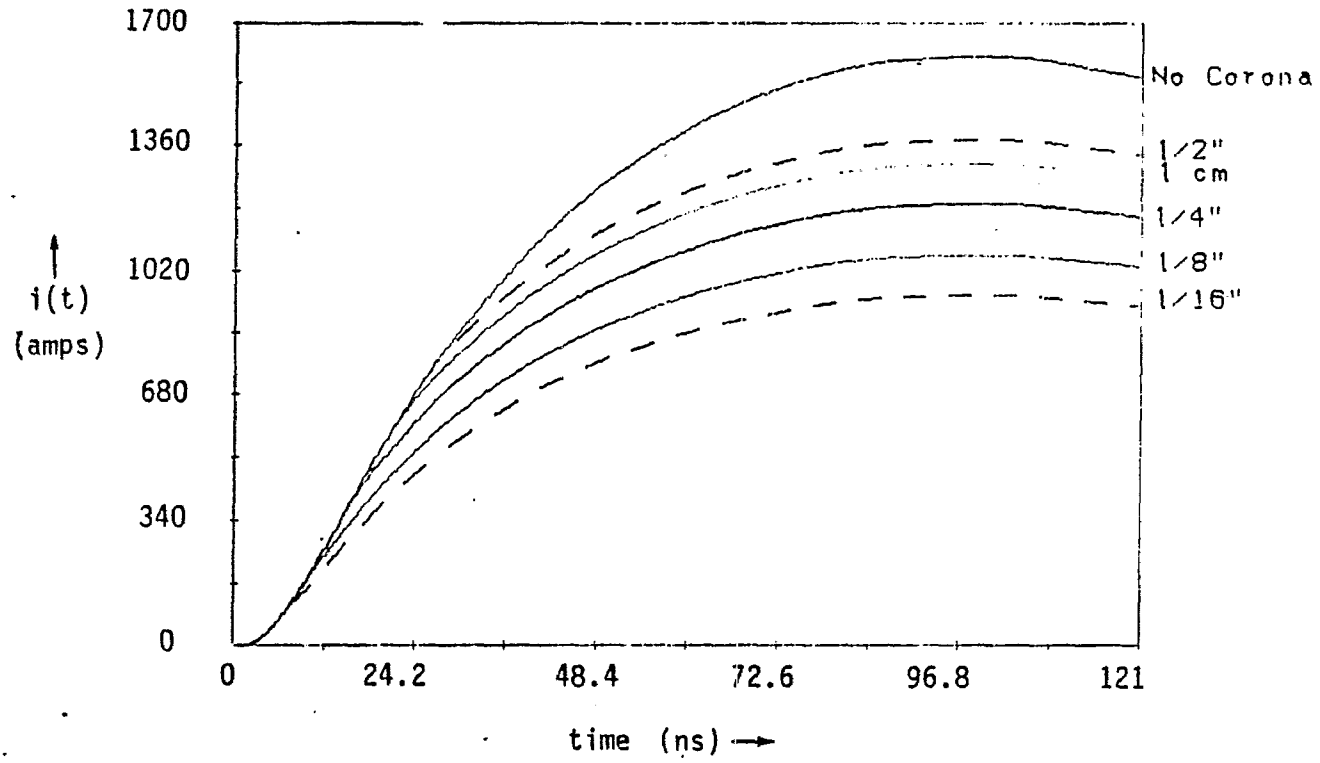

Figure 6a. Late Time Current Response for Varying Wire Radii

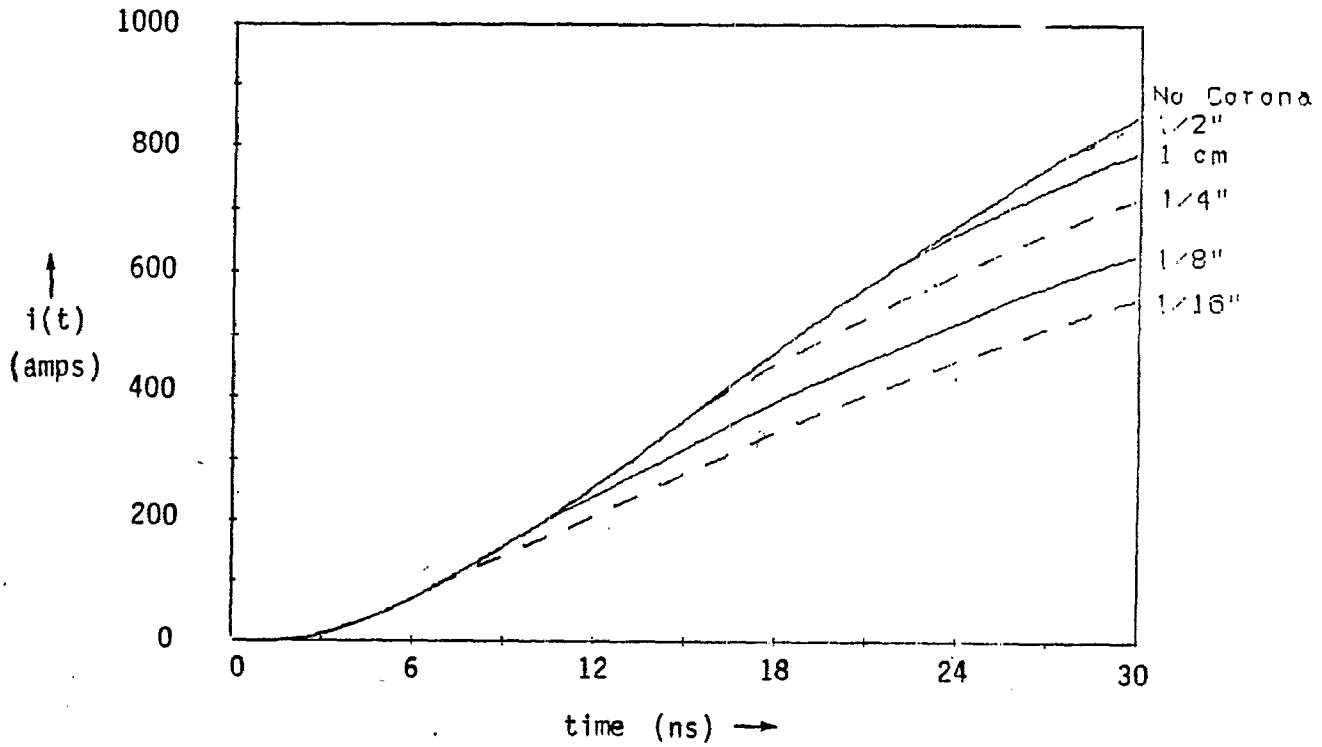

Figure 6b. Early Time Current Response for Varying Wire Radii

C. Parameter f_{g_o}

Baum's model assumes a transmission line model approximating the response of a conducting wire to an incident EMP. When the wire is placed fairly close to a ground plane, the ground plane may serve as the return path for the induced current (i.e. the ground plane is the reference conductor of Figure 1) and the transmission line approximation is reasonable. Calculations of inductance-per-unit-length (L') and capacitance-per-unit-length (C') of the line are straightforward if the line is parallel to the ground plane.

However, analysis of the current induced on a wire in free space by an incident EMP is actually a scattering problem (see [16]). The reference conductor for this geometry may be assumed to be at infinity, but the calculation of per-unit-length inductance and capacitance is not clear. Without appropriate values for L' and C', the use of the transmission line approximation may be ambiguous.

The term f_{g_o} used here gives a measure of the dependence of the transmission line parameters on the geometry of the problem. It has been seen experimentally that the current response of a wire in free space is not especially sensitive to the distance of the reference conductor from the test conductor and that a logarithmic dependence such as that shown in equation (8a) is reasonable for the wire in free space. Other authors [17] have suggested other values for this parameter which may be appropriate. The beauty of the form (8a) is that one may use a logarithmic expansion of the arccosh term in equation (8b) to obtain an approximation of equation (8b) of the same form as equation (8a), with reference conductor radius = 2h (where h = height of test conductor above ground plane) (see reference [12]). It might be noted that in reality most wires "in free space" are actually located above a ground plane.

When the formation of corona is not considered, the per-unit-length current on the wire is given by equation (11):

$$I(\tau) = \left\{-\cos(\alpha) + \frac{1}{\cos(\alpha)}\right\}^{-1} \frac{cE_1 g(\tau)}{Z_0 f_{g_0} \cos(\alpha)} \qquad (11)$$

Note that a change in f_{g_0} directly changes the magnitude of the induced line current. This is illustrated in Figure 7.

Looking at the equation for induced line current when corona formation is considered (equation (12)),

$$\left[-\cos(\alpha) + \frac{1}{\cos(\alpha)} - \frac{\cos(\alpha)}{2\pi f_{g_0}} \ln\left(\frac{Q_0' c}{\cos(\alpha)}\right) + \frac{\cos(\alpha)}{2\pi f_{g_0}} \ln(|I(\tau)|)\right] I(\tau) = \frac{cE_1 g(\tau)}{Z_0 f_{g_0} \cos(\alpha)} \qquad (12)$$

dependence of the line current on f_{g_0} is not immediately apparent. To solve this equation for the current, I(t), one must find the zeroes of an equation of the form:

$$F(X) = (A + B \ln X)\, X - C \qquad (15)$$

where

$$A = -\cos(\alpha) + \frac{1}{\cos(\alpha)} - \frac{\cos(\alpha)}{2\pi f_{g_0}} \ln\left(\frac{Q_0' c}{\cos(\alpha)}\right) \qquad (15a)$$

$$B = \frac{\cos(\alpha)}{2 f_{g_0}} \qquad (15b)$$

$$C = \frac{cE_1 g(\tau)}{Z_0 f_{g_0} \cos(\alpha)} \qquad (15c)$$

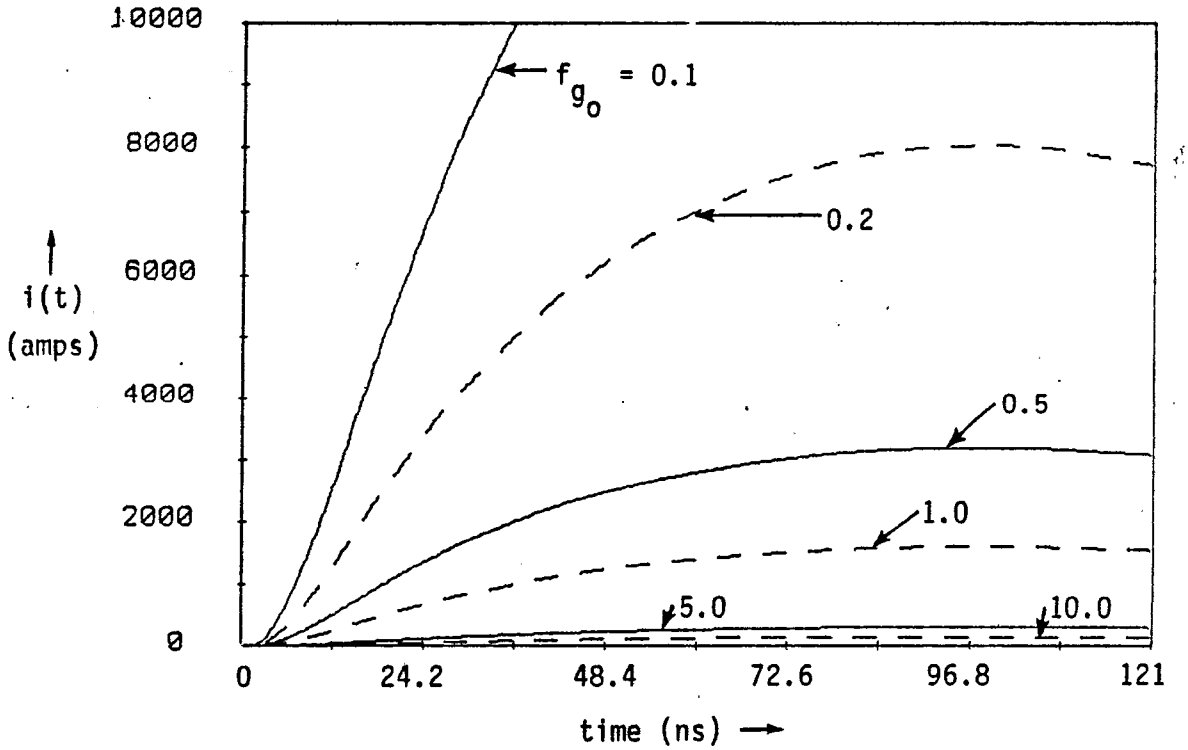

Figure 7. EMP induced line current with varying f_{g_o} - neglecting corona effects.

Setting C=0 for convenience, this equation is plotted as a function of I(t) for various values of f_{g_0} in Figure 8.

It may be seen that for $f_{g_0} \gtrsim 1.3$, the number of roots of the equation go from three to one and the function plot becomes linear. To find out why this is, set equation (15) equal to zero and take the limit as f_{g_0} becomes large. A approaches $\{-\cos(\alpha) + 1./\cos(\alpha)\}$ and B goes to zero. Equation (15) assumes the form

$$\left\{-\cos(\alpha) + \frac{1}{\cos(\alpha)}\right\} X = \frac{cE_1 g(\tau)}{Z_{c_0} \cos(\alpha)} \qquad (16)$$

With $X=I(\tau)$, this is exactly the form of equation (11)! Hence, as f_{g_0} gets larger, this model predicts corona is less and less likely to form. This is shown graphically in Figure 9, where the EMP-induced line current with corona present (dashed line) approaches that without corona (solid line) as f_{g_0} increases.

(Note that f_{g_0} is ill-defined for a wire not parallel to a ground plane. Here, it is assumed the line is parallel to the ground plane at the altitude of the observation point. For wires at a small angle of incidence with respect to the ground plane, this may be a reasonable assumption. The experiment to be performed based upon these calculations will check the validity of this assumption.)

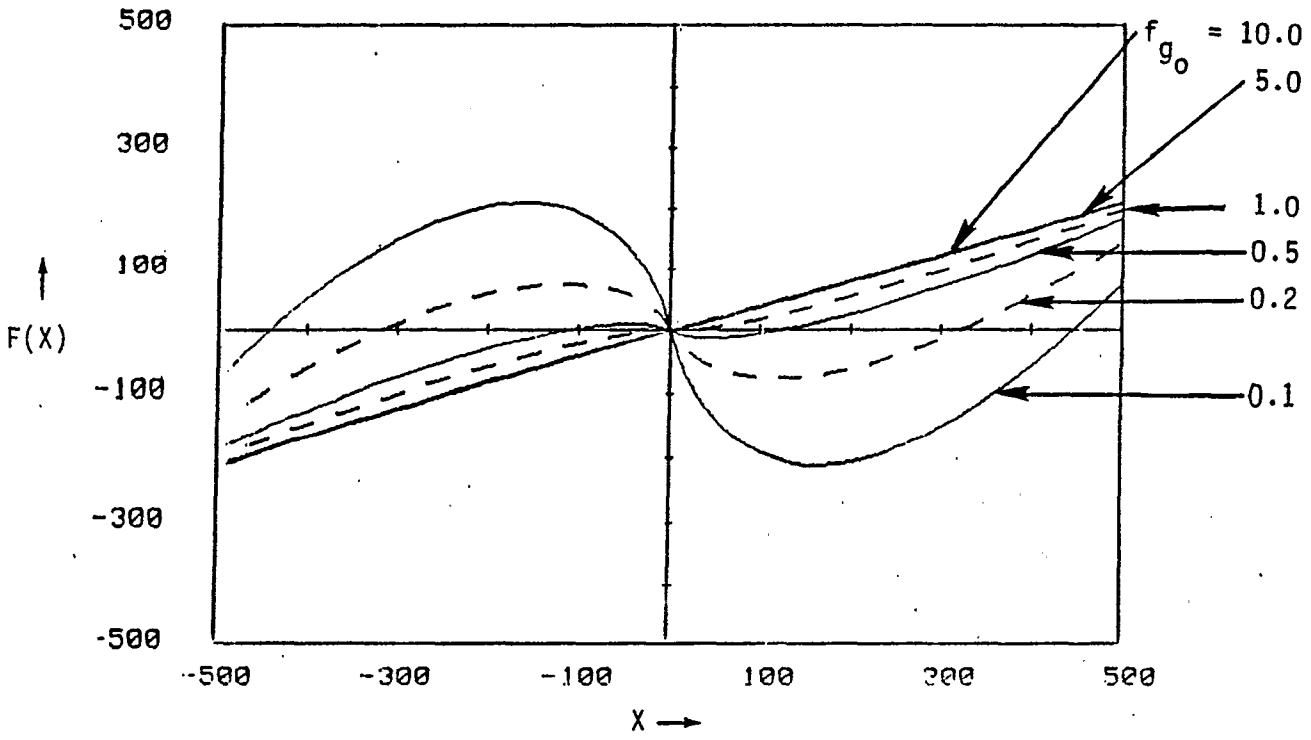

Figure 8. Graph of Corona Response Function

$F(X) = A + B \ln(|X|)*X$

for different values of parameter f_{g_o} .

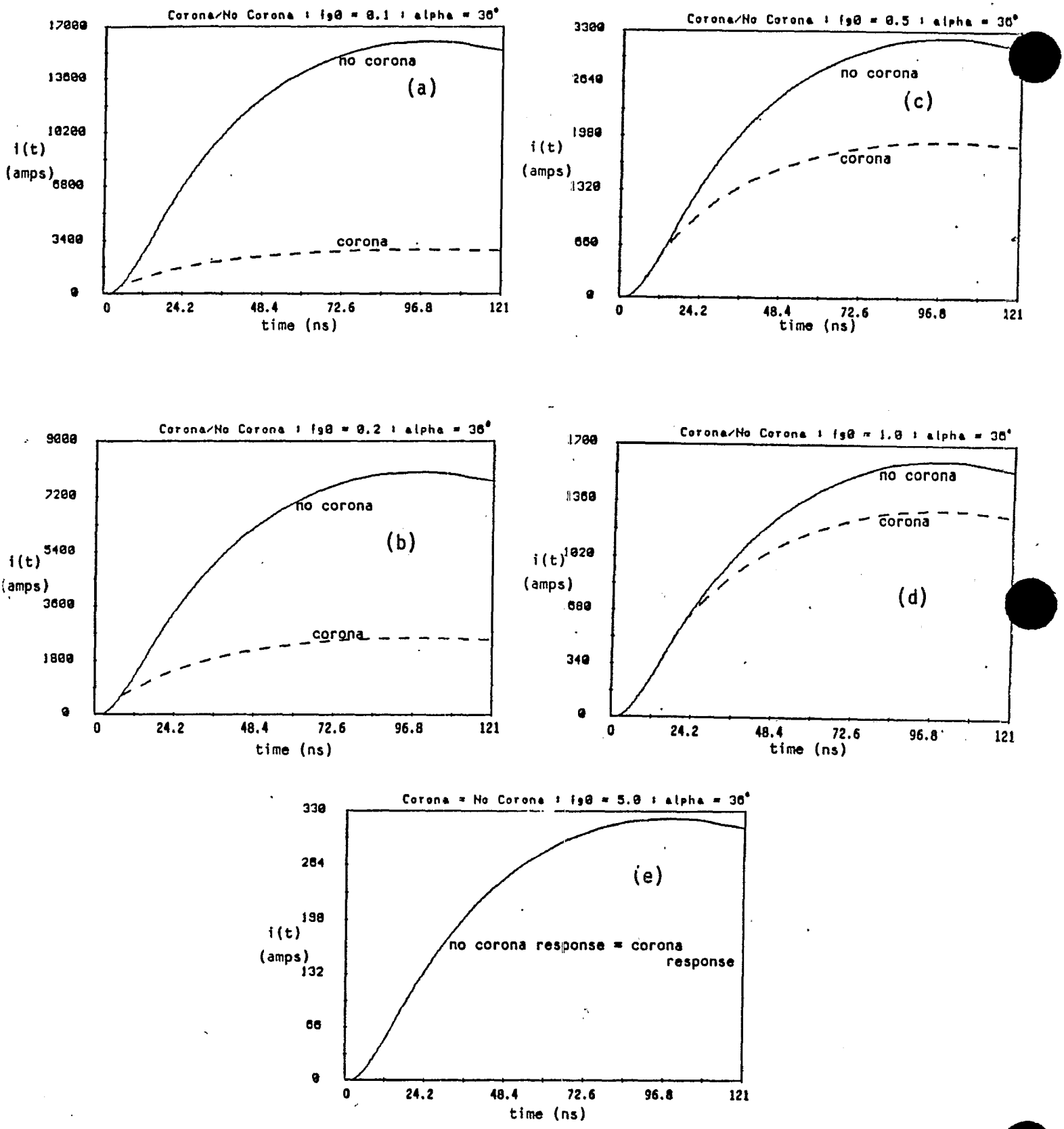

Figure 9. EMP induced line current for several values of parameter f_{g_o} .

D. Angle of Incidence

Figures 10 and 11 show the effects of changing angle of incidence for lines with no corona and with corona assumed, respectively. Notice that a change in the angle of E-field incidence upon the wire has more impact upon the magnitude of current when the formation of corona is NOT assumed. Figure 12 compares the corona with no corona responses of conducting lines for different angles of incidence. (Dashed lines indicate the current expected on the line using the corona model. Solid line curves assume no corona formation.) Although values on the vertical axes vary from graph to graph, the important thing to note is the relative value of corona to no corona response at differing angles of incidence. It is apparent that smaller angles of incidence lead to earlier corona onset and more distinct differences between the expected corona and no corona (i.e. if no corona forms) current responses. Table 3 provides examples of corona onset times as the angle of E-field incidence varies.

ANGLE OF INCIDENCE (deg)	CORONA ONSET TIME (ns)
18	12.8
27	17.1
36	22.5
54	45.2

TABLE 3 : CORONA ONSET TIMES WITH VARYING ANGLE OF INCIDENCE

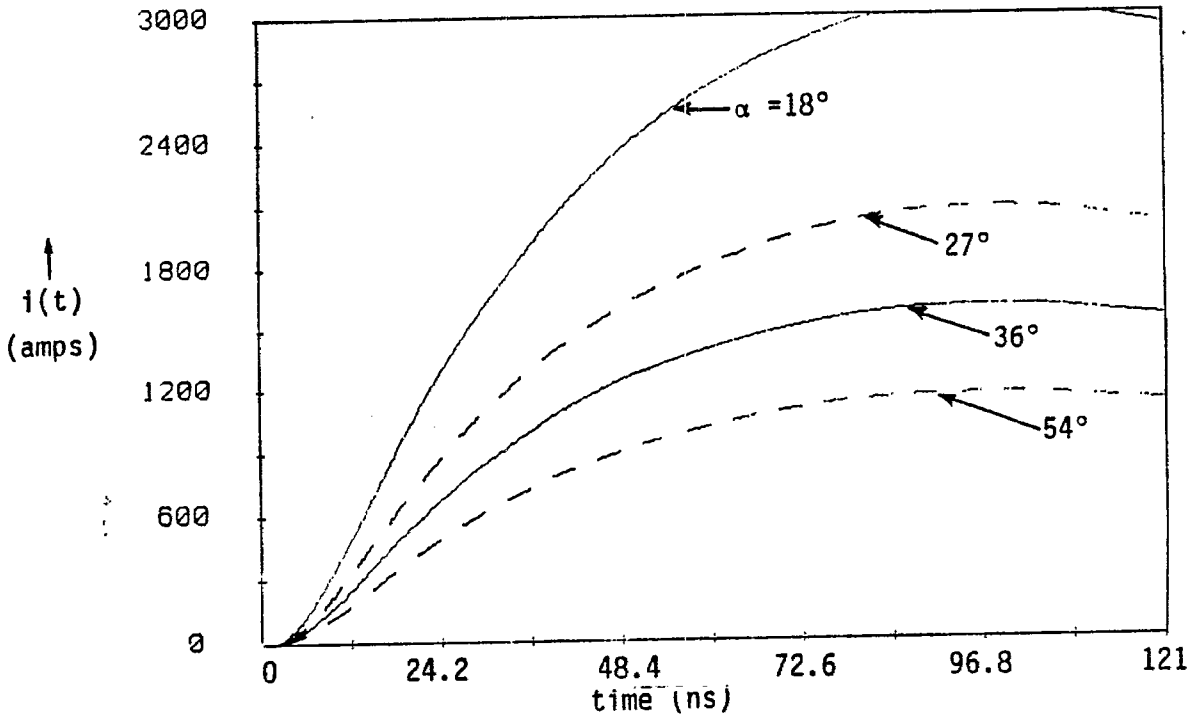

Figure 10. EMP-induced line current for differing angles of E-field incidence---corona effects neglected.

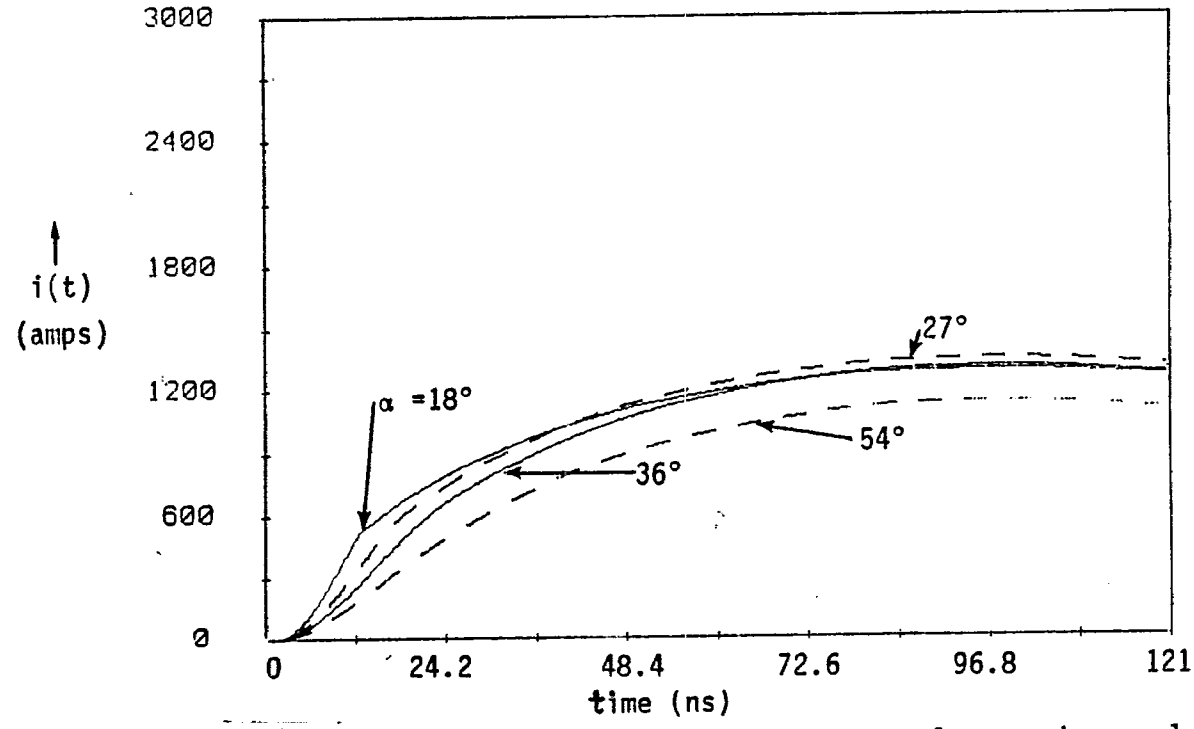

Figure 11. EMP-induced line current with corona for varying angle of E-field incidence

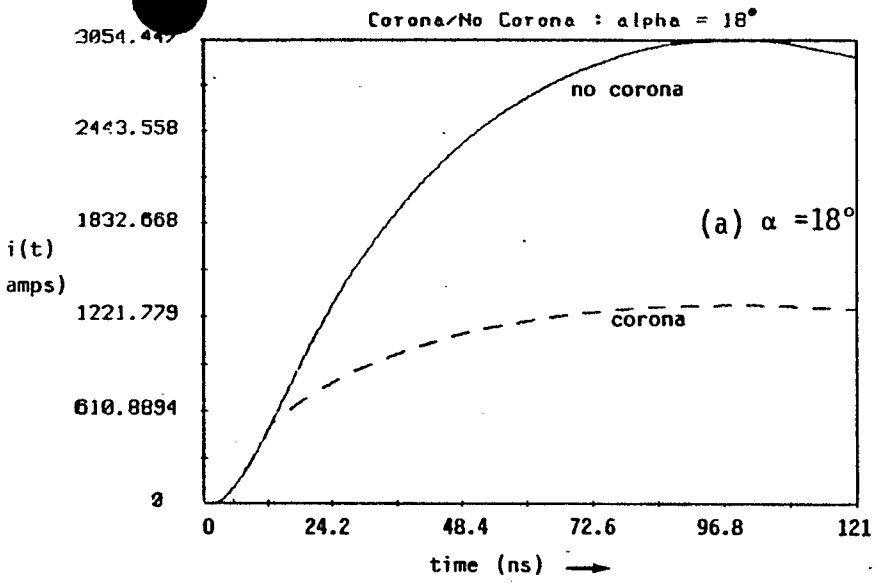

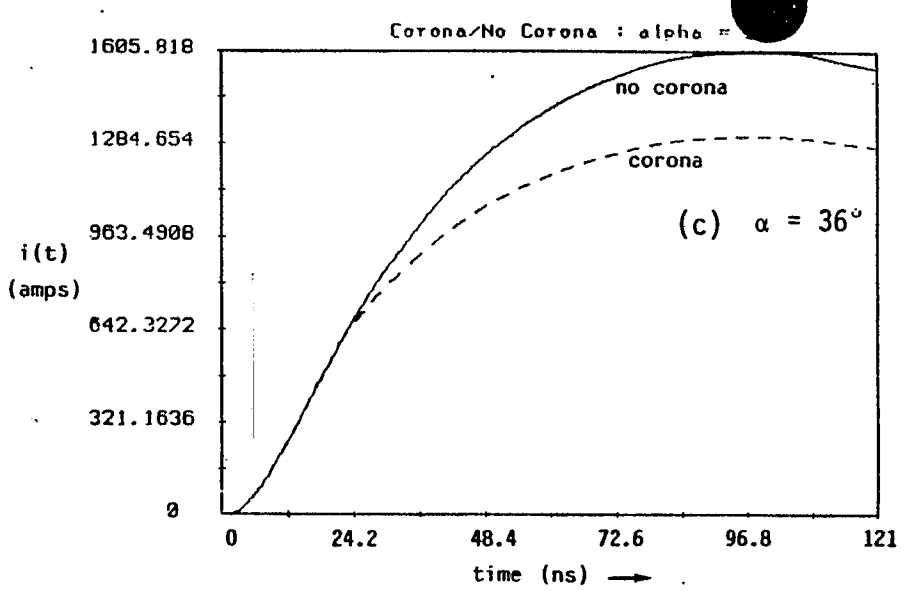

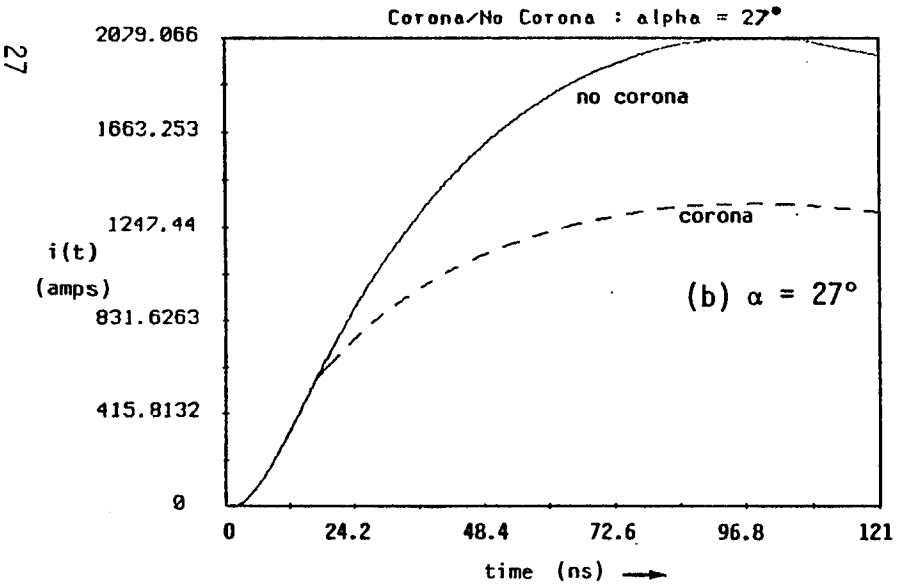

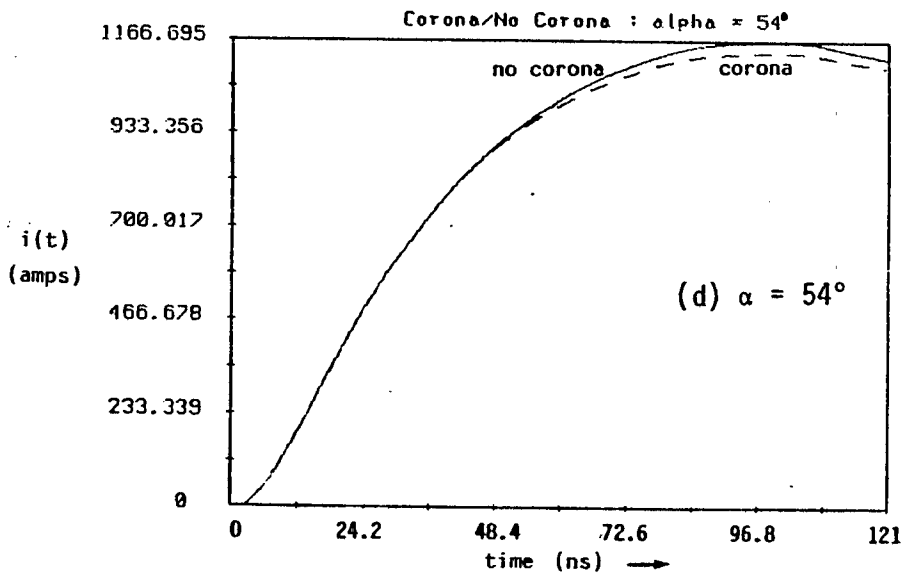

Figure 12. Comparison of EMP-induced line currents for different angles of E-field incidence, α .

V. EXPERIMENTAL LIMITATIONS: CLEAR TIME

Clear time (t_c) is defined as the difference in arrival time between the original signal from the VPD at the observation point and the arrival of any disturbance due to a discontinuity in impedance or experiment geometry (cf. [13]). Possible end effects limiting clear time in the proposed experiment are diagrammed in Figure 13 where path #1 is the direct path of a wave from the base of the VPD to the observation point. A wave from the base of the VPD may also travel slightly above the ground plane and induce a current at the bottom end of the wire that would travel up to the observation point (path #2). Similarly, a wave from the top of the VPD may travel to the observation point via a current induced at the upper wire end (path #3).

Since the clear time limit is determined strictly by the shortest significant interference path, only those paths shown in Figure 13 are considered. Reflections from the ground plane could also limit the clear time of the experiment. However, such scattering paths generally cause only small perturbations in the current response of interest since the magnitude of the incident E-field is reduced in each reflection. Current reflections arising from impedance discontinuities at the line ends are much more important in the determination of clear time limits. These are diagrammed in Figure 14. The current induced at the observation point may travel down the line and be reflected at the ground end back to the observation point (path a) or it may travel up the line towards the VPD and be reflected back to the observation point (path b). Comparing Figures 13 and 14, path #2 is always shorter than path a (as the observation point gets closer to the ground, the length of path #2 approaches that of path a) and path #3 is always shorter than path b.

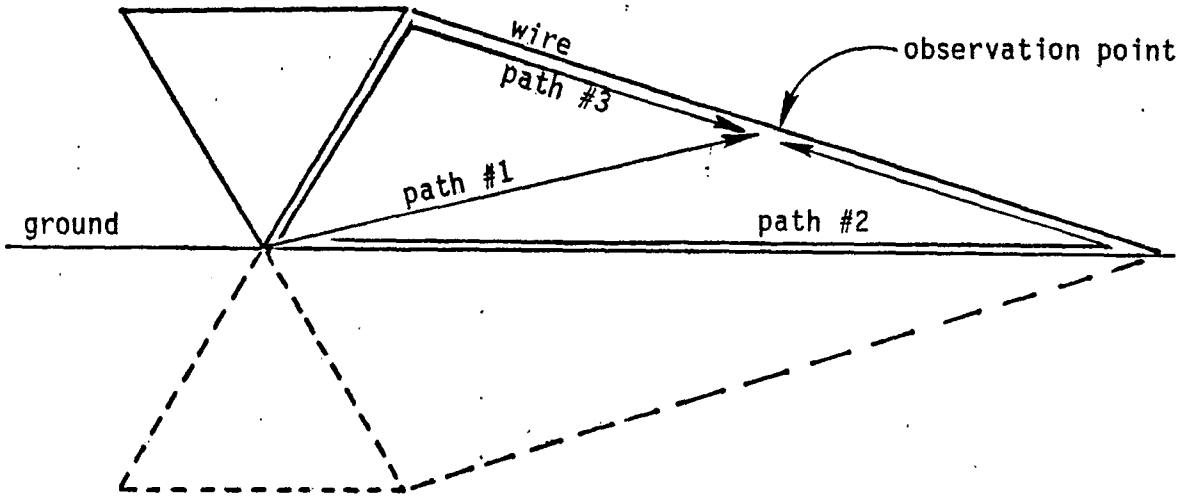

Figure 13. Possible End Effects Limiting Experiment Clear Time

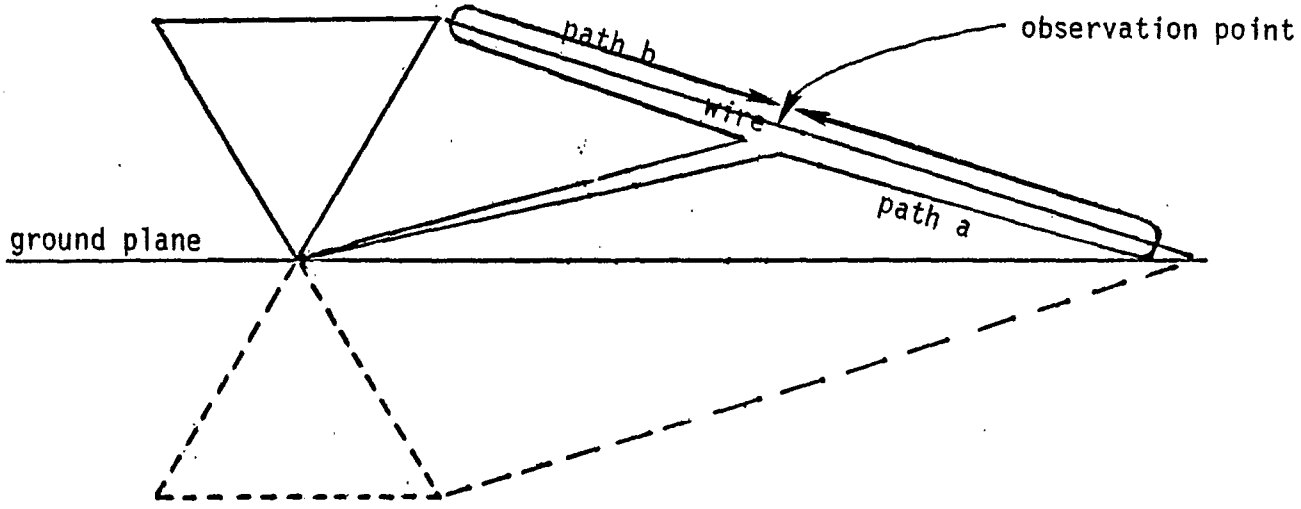

Figure 14. Current reflections from impedance discontinuities at line ends

Using the geometry of Figure 13, maximum clear times are calculated for varying lengths of conducting test wire. Maximum clear time is defined as follows: The minimum of paths (#2-#1) and (#3-#1) (i.e. the relative lengths with respect to the most direct path from the chosen observation point) is found for many possible observation points sampled along a given length of line. The maximum of these minimum paths (there is one minimum path for each sample observation point) is chosen for the given line length and is converted to units of time by multiplication by 1/c (where c = speed of light). This gives the optimum clear time (and, from the coordinates of that path, the best observation point) for a given conducting wire length. The results of these calculations are graphed in Figures 15 and 16 for possible wire lengths between 40 and 145 meters. Maximum clear time versus wire length is shown in Figure 15 while optimum observation point (as measured from the lower wire end) is plotted against wire length in figure 16.

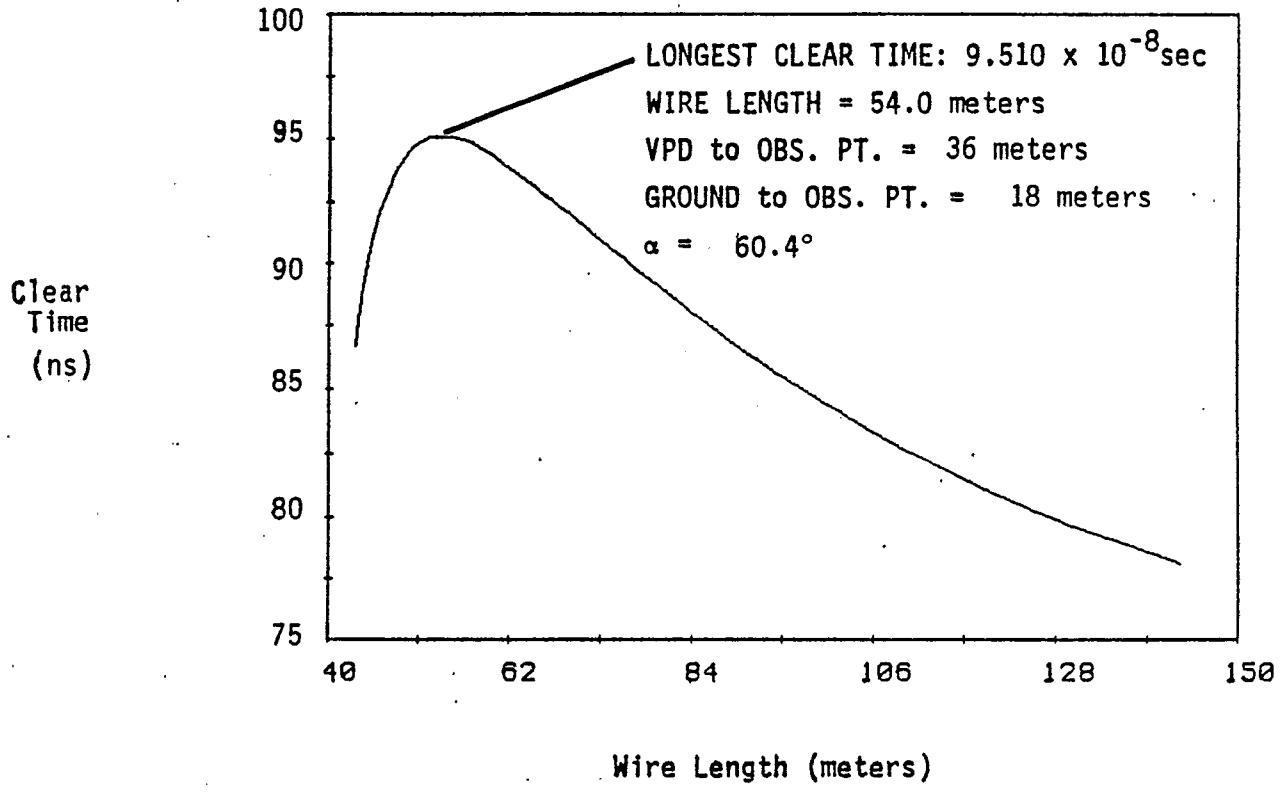

Figure 15. Clear Time vs. Wire Length

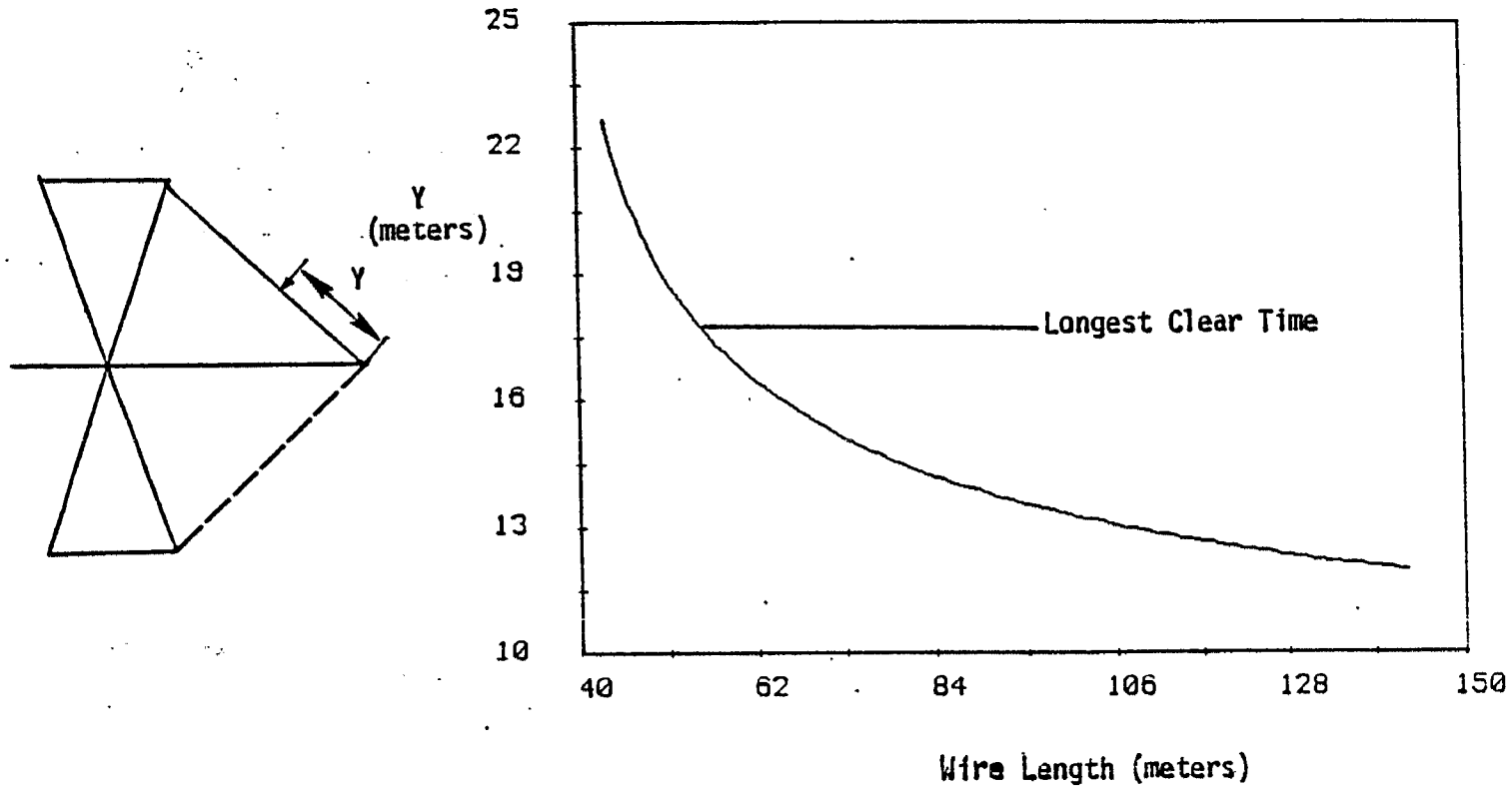

Figure 16. Optimum Observation Point Distance from lower wire end, Y, vs. Wire Length.

Unfortunately, at the optimum observation point on a wire 54 meters long (i.e. obtaining maximum clear time), the angle of E-field incidence with the wire is 60.4°. As discussed earlier, the difference between expected current values with and without corona is not as distinct at this angle as for smaller angles of incidence. In fact, corona effects may not appear before clear time limitations are encountered.

As the test wire becomes longer than 54 meters, the clear time, angle of incidence, and the magnitude of $E_1 g(\tau)$ at the observation point with optimum clear time for that wire length grow smaller. Figure 17 indicates the expected current as a function of time for different lengths of wire. Appropriate local angle of incidence, local magnitude of E-field, local f_{g_0} estimate, and a constant test wire radius of 1 cm are used for each set of curves, so the results are more realistic than those of section IV. (Again, solid lines indicate response with no corona and dashed lines indicate the expected response if corona formation is assumed.). Notice that the results for a wire 50 meters long show no difference between the corona and no corona responses. This case is very close to that of the optimum clear time case mentioned above. As the wire becomes longer, the angle of incidence decreases as does as the magnitude of the local E-field. The decrease in angle of incidence can be seen in the larger difference between no corona and corona responses. In all cases, the local value of $E_1 g(\tau)$ is sufficient to cause corona. (For these calculations, a test wire radius of 1 cm was used.) A dark bar below the horizontal axis indicates the clear time expected for each case considered.

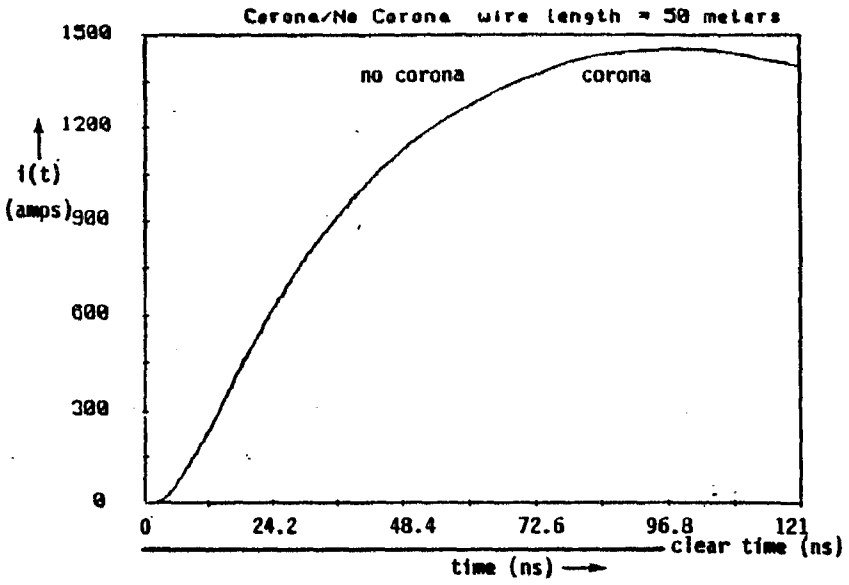

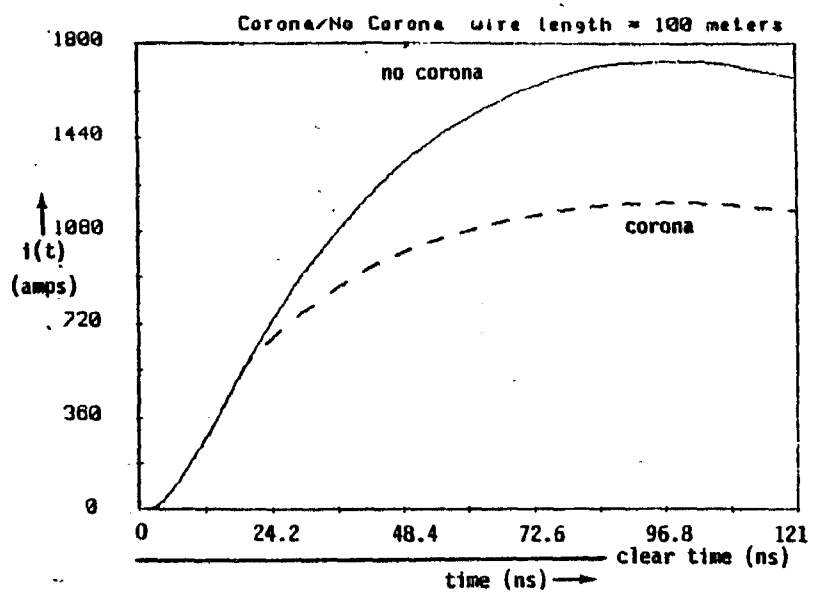

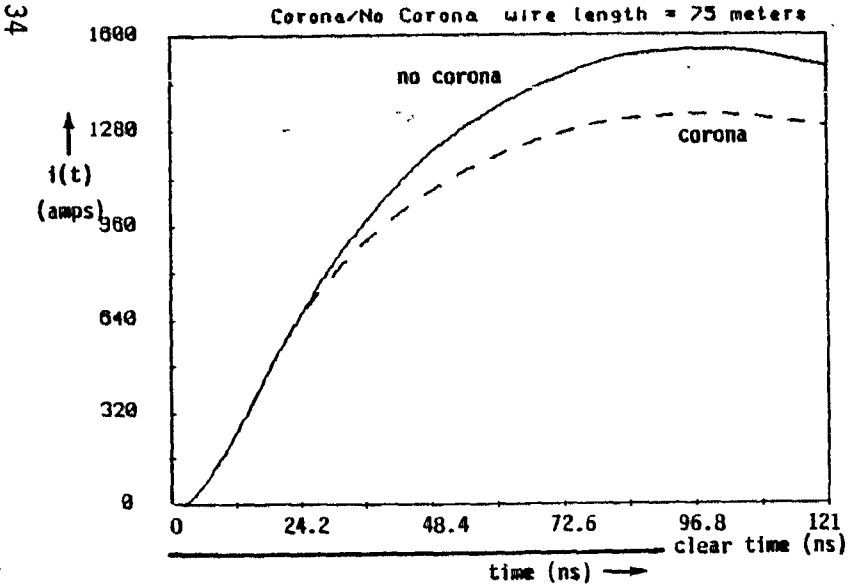

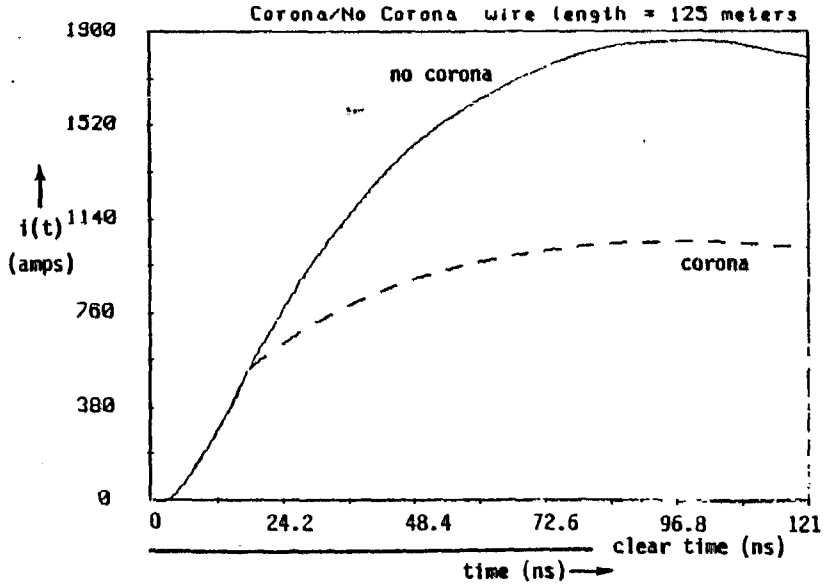

Figure 17. EMP-induced Current vs. Time for Different Lengths of Test Conductor Lines.

VI. SUMMARY

From the preceding discussion, it is apparent there is a trade-off to be made among many parameters: test conductor radius, f_{g_o}, magnitude of local E-field, angle of incidence, wire length, and clear time. These are summarized in the table below:

PARAMETER	IDEAL FOR MAXIMUM CORONA	CONFLICTING LIMITATIONS
wire radius	small	must be able to hold EG&G OMM i current probe
f_{g_o}	small-- less than ~ 1.3	geometric constraints on experiment; not well defined
local E-field	large; $E \geq E_b$	an otherwise optimum observation point may be too far from source
angle of incidence	small, but not 0°	if too small, observation point may be too far from source (E-field too small)
wire length	long to get small angle of incidence; short to get larger E-field and longer clear times	longer wire is more expensive and heavier (harder to keep known angle of incidence)
clear time	longest possible	optimum clear time for chosen geometry yields too large an angle of incidence.

TABLE 4 : ANALYSIS OF PARAMETERS IN CORONA MODEL

Some of these restrictions are not as critical as others. It has been shown that at the optimum observation point for maximum clear time, there is not much difference between the current response expected when corona is present and when it is not. Figure 15 indicates there is a reasonable amount of clear time for other lengths of test wire, so it is not essential to use that optimum position.

A longer test wire seems to be better. The local angle of incidence at the optimum observation point would be smaller. The value of the parameter f_{g_0} would be smaller since the observation point would be closer to the ground, and the definition chosen for f_{g_0} is more likely to be correct since the wire would be closer to parallel to the ground plane. There are limits to this: The wire cannot be so long as to put the observation point outside the region where the local E-field is sufficient to cause corona before clear time limitations set in.

Restrictions on wire radius seem to be related to the current probe manufacture. Although conductor wire radius does have an impact on corona onset time, the expected clear times are almost an order of magnitude larger than the corona onset time differences. Nevertheless, the minimum possible wire radius should be chosen to increase the time corona effects are observed.

Combining all of these effects, except variation in wire radius, a more realistic picture of expected experiment results emerges. Figures 18a-e show the values of different parameters plotted as a function of wire length for the experiment geometry described above. In general, the only default value used was setting the wire radius equal to 1 cm.

Figure 18a shows the local E-field correction necessary at the optimum observation point (obtained from Figure 16) for varying wire lengths. This correction is applied to the default E-field shown in figure 5. The curve shown is not exactly linear since, as indicated in figure 16, the location of the optimum observation point is not linear with wire length.

Variation in f_{g_0} as a function of wire length is shown in Figure 18b where the wire is assumed to be locally parallel to the ground plane at the optimum observation point for the given wire length. This approximation becomes more realistic for increasing wire lengths. This graph also shows that for increasing wire lengths the default f_{g_0} value of 1.0 used earlier is reasonable.

Figure 18c demonstrates the changing local angle of E-field incidence with wire length. Since smaller angles of incidence yield greater distinctions between corona and no corona responses, it is clear from this graph that a longer test wire is preferred.

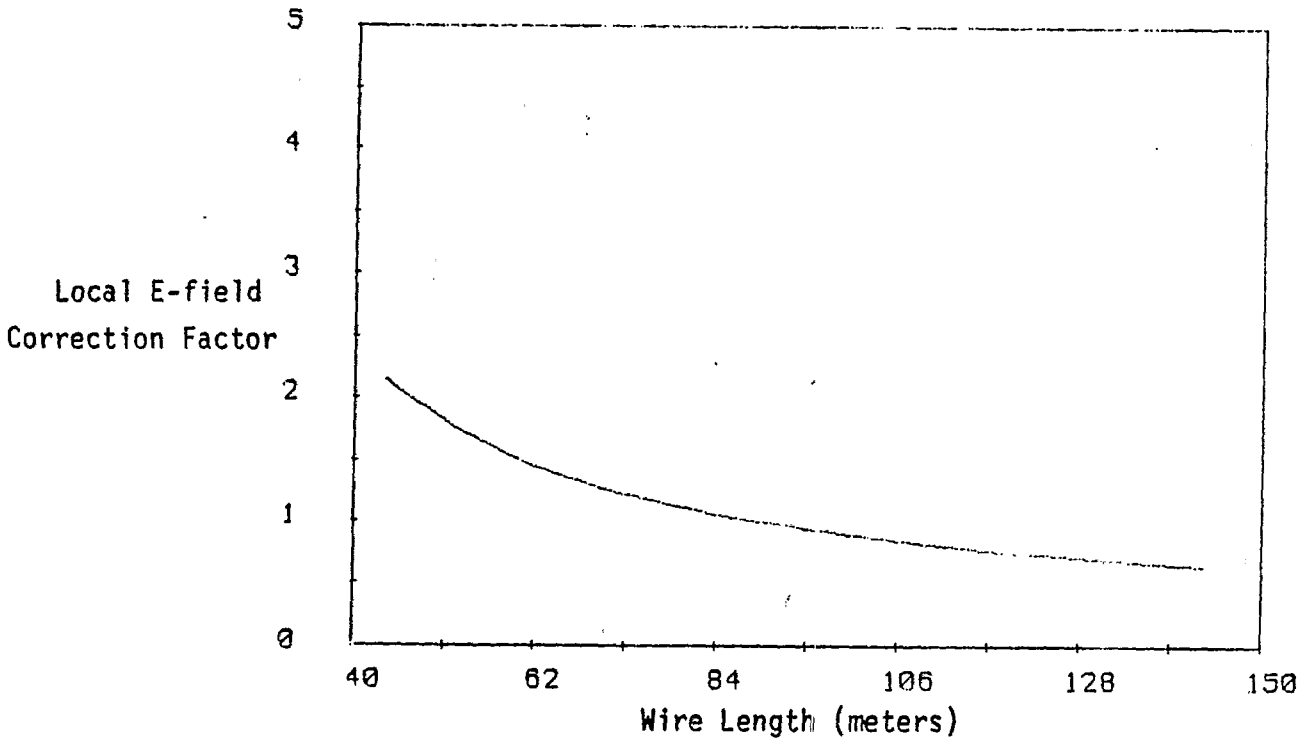

Figure 18a. Local E-field Corrections as Function of Wire Length.

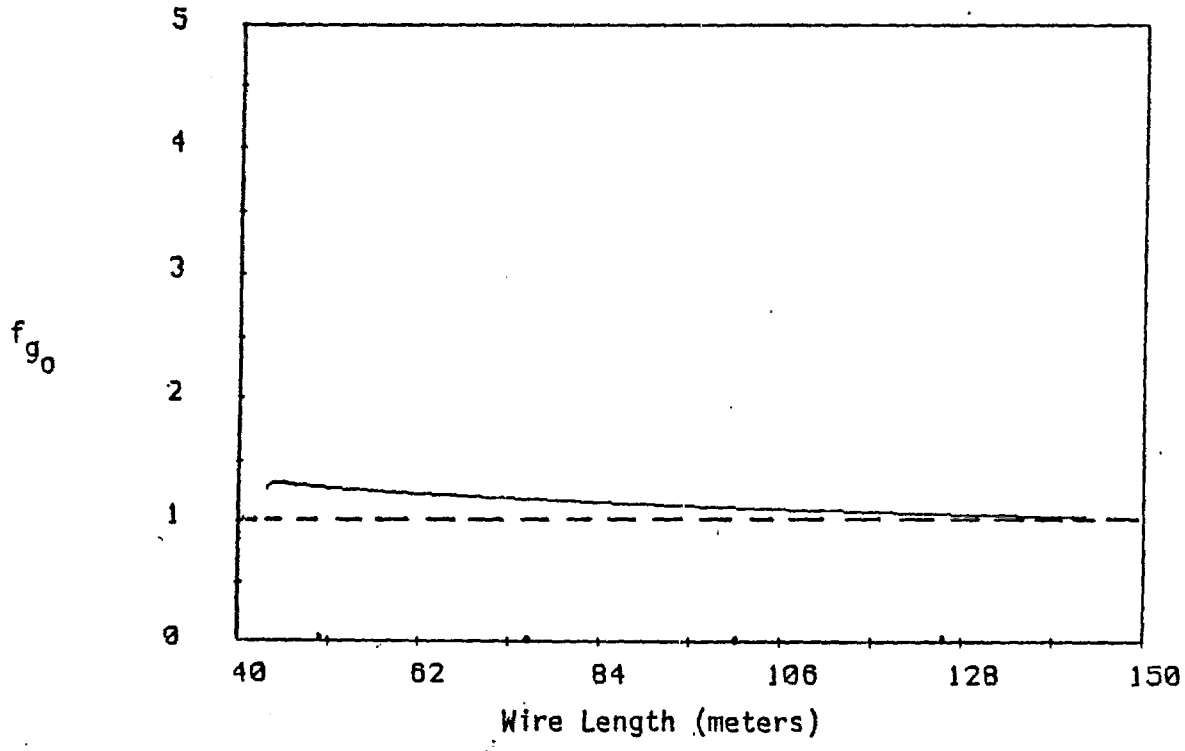

Figure 18b. f_{g_0} as Function of Wire Length

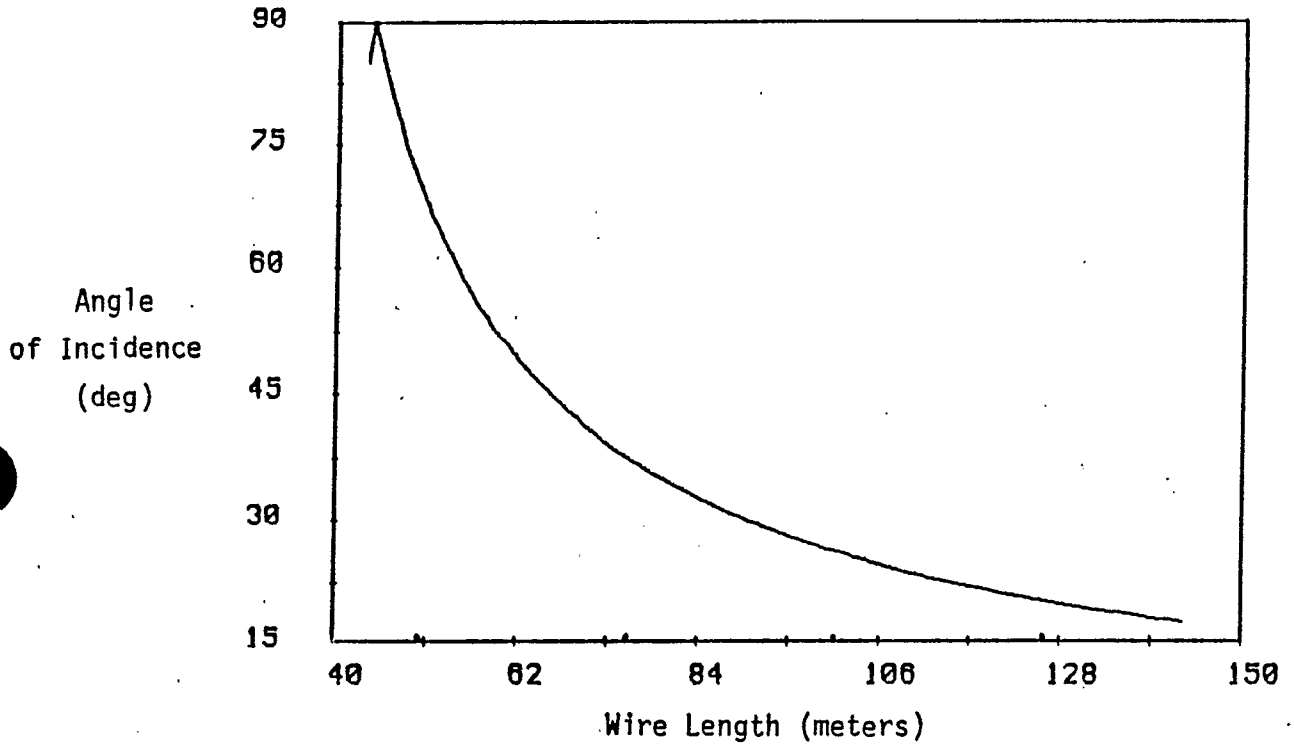

Figure 18c. Angle of E-field of Incidence at Optimum Observation Point as Function of Wire Length.

When each of these variations is taken into consideration, corona onset time changes. This is demonstrated in Figure 18d (In all curves shown in this plot, increasing wire length is synonymous with decreasing angle of E-field incidence with the wire.)

Curve a of Figure 18d takes into consideration only the variation in local angle of E-field incidence (Default values of E_0 and f_{g_0} from Table 1 are used). The results plotted here are consistent with Table 3. Curve b includes the effects of declining E-field with distance, but retains the default value for f_{g_0}. Curve c uses a local calculation of f_{g_0} appropriate for the height above ground of the optimum observation point on the line but retains the default E-field values. Finally, curve d combines all of these effects (using only the default value of wire radius = 1 cm) to give the most realistic plot of expected corona onset times.

In Figure 18e, the results plotted in curve 18d-d are subtracted from the clear time curve of figure 15 to give total expected length of clear time (or "clear time window") for wire lengths between 40 and 145 meters.

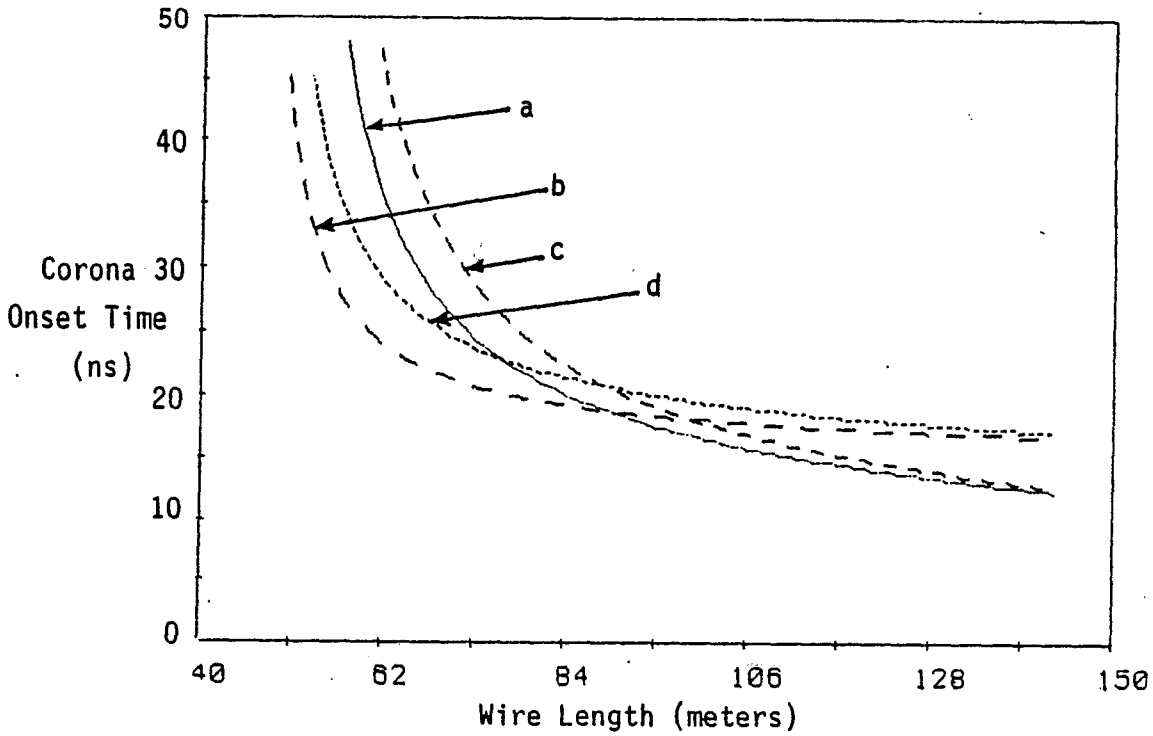

Figure 18d. Comparing Effects of E-field and f_{g_0} change with wire length.

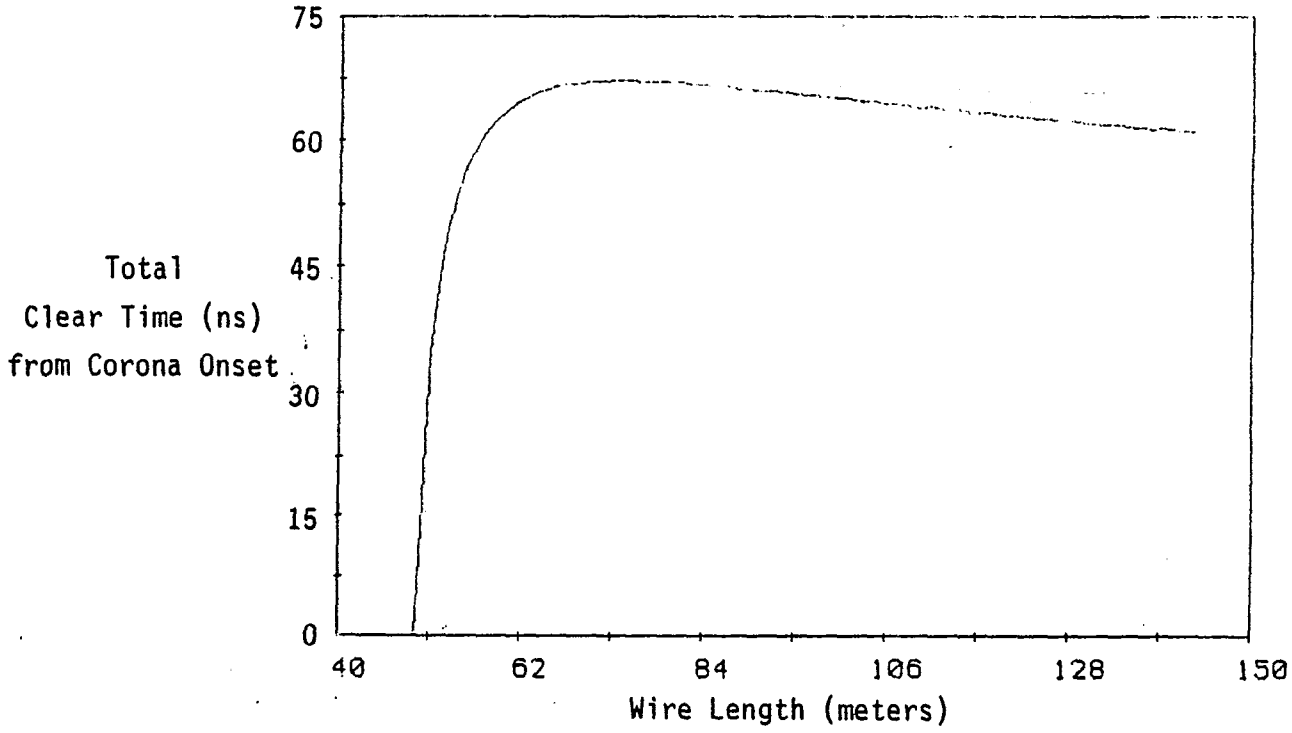

Figure 18e. Clear Time Window as a Function of wire length.

Many assumptions are made in this model that may be invalidated by experiment. The wave incident upon the test conductor is assumed to be (at least locally) planar. In fact, waves from the VPD are spherical. At sufficient distances from the VPD the plane wave assumption may be reasonable.

The onset of corona is assumed to be immediate. In fact, the air chemistry involved in the generation of corona occurs in a finite time after a normal E-field of magnitude larger than the breakdown strength of air is attained. If this time is much much less than the corona onset times calculated, it may be considered negligible, as it was in this model.

Variations in air pressure and moisture may effect the breakdown strength of air. The value chosen for these calculations (3×10^6) may be conservative. Other authors [11] have used half this value in their calculations. Since the experiment is expected to be conducted at the VPD facility near Albuquerque, New Mexico where the air is drier and less dense, the lower value may be more appropriate. Notice that a smaller value of E_b would lead to earlier corona onset. Hence the calculated corona onset times shown here may be conservative.

A test conductor which is not smooth may exhibit local variations in corona (i.e. more corona at sharper points). If the wire is not exactly straight, both the local corona and angle of incidence will be changed. It will be necessary in the experiment to minimize the sag in the line.

Clear time calculations assumed waves travelling at the same speed on the VPD, in air, and on the line. If there are significant differences between the actual speeds, the clear times calculated will be inaccurate.

VII. CONCLUSIONS

An experiment geometry (as diagrammed in Figure 4) is postulated to test corona effects due to EMP fields incident on a conducting wire based upon a corona model first described by Baum [11]. After analysis of the parameters of this model, as well as experimental limitations, a test wire longer than 75 meters would seem best for observation of corona. Wire lengths shorter than 75 meters imply a more ill-defined f_{g_o}, increasing angles of incidence, and delayed corona onset times.

From Figure 18e, it is apparent that clear time will continue to decrease with longer lines. (This may also be seen in the diagram of Figure 13 where the length of path #1 approaches that of path #3 for longer test conductor wires.) In addition, the magnitude of the local E-field continues to fall of beyond this point, implying later corona onset times. However, it has been shown that for wires up to 125 meters in length, a distinction between corona and no corona responses is still apparent.

A number of other restrictions also put a general upper bound on the length of the wire which are hard to quantify at this time. Among them are cost constraints (for wire and supports), weight limitations on the wire, and area in which to perform the experiment. These will be studied and discussed further as experiment design continues.

VIII. REFERENCES

1. Peek, F.W., Jr., Dielectric Phenomena in High-Voltage Engineering, McGraw Hill Publishing, New York, 1929.

2. Cobine, J.D., Gaseous Conductors, Dover Publications, New York, 1941.

3. Wagner, C.F. and B.L. Lloyd, "Effects of Corona on Travelling Waves", Transactions of the American Institute of Elect. Engineers, Power Apparatus and Systems, Vol. 74, October 1955, pp. 858-872.

4. Lam, J., "Theoretical Study of the Electrical Corona on a Long Wire", EMP Interaction Note #305, Air Force Weapons Laboratory, Albuquerque, NM, June 1976.

5. Chen, K.C., "Transient Corona Effects on a Wire over the Ground", Proc. Lightning Technology, NASA Conf. Pub. 2128 and FAA-RD-80-30, April 1980, pp. 265-281.

6. Book, P.S. and H.J. Price, "A Transmission Line Corona Experiment", EMP Interaction Note #313, Air Force Weapons Laboratory, Albuquerque, NM, October 1976.

7. Book, P.S., "Study of Corona in a Transmission Line Test Facility", EMP Interaction Note #369, Air Force Weapons Laboratory, Albuquerque, NM, November 1978.

8. Baum, C.E., "Return Stroke Transmission Line Model", Lightning Phenomenology Note 12, October 1981.

9. Baum, C.E., "Properties of Lightning Leader Pulses", Lightning Phenomenology Note 2, December 1981.

10. McConnell, B.W. and P.R. Barnes, "A Preliminary Assessment of the Impact of the Electromagnetic Pulse on Electrical Power System Insulation", Gaseous Dielectrics IV, Proc. of the Fourth International Symposium on Gaseous Dielectrics, Knoxville, TN, April 29 - May 3, 1984, Pergamon Press.

11. Engheta, N., K.S.H. Lee, F.C. Yang, and R. Aguero, "High Altitude Electromagnetic Pulse (HEMP) Interaction with Transmission and Distribution (T&D) Lines: 1. Corona Effects on Induced Transients 2. Induced Stresses in Insulators", Dikewood Memo, January 1985.

12. Baum, C.E., "Effect of Corona on the Response of Infinite-Length Transmission Lines to Incident Plane Waves", EMP Interaction Note #443, Air Force Weapons Laboratory, Albuquerque, NM, February 1985.

13. Kehrer, W.S. and C.E. Baum, "Electromagnetic Design Parameters for ATHAMAS II", Athamas Memo #4, Air Force Weapons Laboratory, Albuquerque, NM, May 1975.

14. Singaraju, B.K., C.E. Baum, and J.H. Darrah, "Design Improvements Incorporated in ATHAMAS II (Larger VPD)", Athamas Memo #11, Air Force Weapons Laboratory, Albuquerque, NM, January 1976.

15. Handbook of Chemistry and Physics, 58th edition, CRC Press, Inc., Cleveland, OH.

16. Barnes, P.R., "The Axial Current Induced on an Infinitely Long, Perfectly Conducting, Circular Cylinder in Free Space by a Transient Electromagnetic Plane Wave", EMP Interaction Note #64, Air Force Weapons Laboratory, Albuquerque, NM, March 1971.

17. Schelkunoff, S.A., "Concerning Hallén's Integral Equation for Cylindrical Antennas", Proceedings of the I.R.E., December, 1945, pp. 872-878.